UILU-ENG 89-3604

Report No. 150

THE EFFECT OF CASTING POROSITY ON THE FATIGUE LIFE OF LOST-FOAM CAST IRON AND ALUMINUM-SILICON 319

by

Anthony J. Biell IV and Frederick V. Lawrence, Jr.
Department of Materials Science and Engineering

A Report of the

MATERIALS ENGINEERING—MECHANICAL BEHAVIOR

College of Engineering, University of Illinois at Urbana-Champaign

August 1989

ABSTRACT

The fatigue and monotonic properties of a nodular cast iron, gray cast iron, and Aluminum-Silicon 319 cast using the empty-cavity and the lost-foam processes were determined. The cast iron tests were performed at room temperature while the aluminum-silicon specimens were tested at room temperature at 99% humidity and at 300 °F. Fatigue cracks in the nodular cast iron and Aluminium-Silicon always initiated at the largest casting flaw Initial flaw sizes were measured using a scanning electron microscope and used to calculate the initial stress intensity factor, ΔK_o. There is a better correlation in the nodular cast iron and the aluminum-silicon alloy between the initial stress intensity factor of the initiating flaw and the fatigue life than with the maximum stress. There is a better relationship in the gray cast iron between the maximum stress (R = 0.1) and the fatigue life than was observed for the nodular cast iron tests. The role of internal casting porosity was quantified using a linear-elastic fracture mechanics (LEFM) model for fatigue crack growth. The predicted lives agreed with measured values within a factor of two. The nodular cast iron predictions were increasingly conservative at long lives.

ACKNOWLEDGEMENTS

This investigation was conducted in the Materials Engineering Research Laboratory and the Newmark Civil Engineering Laboratory, Department of Civil Engineering, at the University of Illinois, Urbana. It was funded by the General Motors Technical Center, Warren, Michigan under the guidance of Dr. Chhotu Patel, Dr. Dale Gerald, Mr. Kenneth Martin and Mr. Chester Rivard.

I would like to express my sincere appreciation to Professor Frederick V. Lawrence, Jr. for his guidance and support throughout my masters program. Professor Lawrence provided many interesting hours of conversation on topics ranging from engineering to music.

Dr. Grzegorz Banas, Dr. Peter Kurath and Professor Darrell Socie are gratefully acknowledged for their suggestions and assistance with this thesis. Mr. Aslak Siljander is recognized and appreciated for his work on the Aluminum-Silicon testing and analysis. Miss Jill Oderio and Mr. Michael Conlon made valuable contributions in the preparation and testing of the specimens.

My colleagues; Chih-Hsien Ting, Mohammed H. Swellam and Kathleen Holloway are each recognized for the role they played in my technical and cultural development. I would like to thank Dr. Kenneth Packer of Packer Engineering who strongly encouraged me to pursue graduate school.

I would also like to thank my parents, Anthony and Sandra Biell, for their support and encouragement throughout my life. Finally, I would like to thank my fiance, Sheila Anne Wall, for her continued patience, support and sacrifice throughout my graduate studies.

TABLE OF CONTENTS

LIST OF SYMBOLS

a	Crack depth (mm)
a_0	Initial crack depth (mm)
a_f	Final crack depth
ac	as-cast
a/c	Aspect ratio (dimensionless)
c	Half of the surface crack length (mm)
C	Crack growth Coefficient (length/cycle)
C*	Correction factor (dimensionless)
C_1	Correction factor (dimensionless)
C_2	Correction factor (dimensionless)
C_3	Correction factor (dimensionless)
C_4	Correction factor (dimensionless)
da/dN	Crack growth rate (length/cycle)
f	Fatigue test frequency (10 Hz)
$g(\varphi)$	Correction factor (dimensionless)
g(W)	Correction factor (dimensionless)
K_Q	Fracture toughness (MPa)
K_{Imax}	Maximum stress intensity factor
K_{Imin}	Minimum stress intensity factor
ΔK_I	Change in stress intensity factor
ΔK_o	Initial stress intensity factor (calculated using the initial flaw depth)
m	Crack growth exponent (dimensionless)
N	Number of cycles
N_f	Number of cycles to failure (separation of specimen)
Φ	Elliptical integral
φ	angle (taken to be equal to zero in this report)
R	Load ratio (dimensionless)
σ	Stress (MPa); 1 ksi = 6.895 MPa
σ_{max}	Maximum stress (MPa)
σ_{min}	Minimum stress (MPa)
$\Delta\sigma$	Stress range (MPa)
Y_1	Mode I geometry correction factor (dimensionless)

1. INTRODUCTION

Metal Casting can be considered a unique and important forming process for a variety of reasons. One of the most important is the capability of producing complex components in any metal ranging from less than an ounce to single parts weighing several hundred tons [1]. An additional advantage of casting is that it is possible to economically produce extremely intricate shapes by the millions. As a result, the industry has grown to where it is now estimated that castings are used in 90% or more of all manufactured goods and in all capital goods machinery used in manufacturing [2].

Two types of processes are now widely in use in the automotive industry: conventional molding processes (empty cavity, green sand, shell, flaskless molding) and the evaporative pattern casting, often referred to as lost foam casting. The empty cavity technique compacts sand around a pattern that must be removed before pouring the molten metal. The lost foam technique is relatively new (the first patent being issued in 1958) and therefore will be explained in greater detail.

The Lost Foam Casting Process

The first critical step in the lost foam process is to produce a high-quality polystyrene foam pattern. The foam pattern is then prepared for casting by attaching it to a gating system (often molded as part of the pattern) of material of the same type and density. The pattern system with the gating is then coated inside and out with a permeable refractory coating. Once the coating is dry, the pattern system is ready for investment into a one-piece sand flask. Investment of the pattern is achieved by positioning the pattern system in the flask, which has a bed of sand in the bottom of the flask.

Once the pattern system is properly positioned, loose, unbonded sand is introduced in and around it. The flask is vibrated to allow the loose sand to flow and compact in and around all areas of the pattern. When compacting is complete, the flask is moved into the pouring area, and molten metal is poured into the pouring basin. The metal vaporizes the foam pattern, precisely duplication the intricacies of the pattern. After the casting cools, it is then ready for degating and cleaning. See references 3-5 for a more detailed explanation of the lost-foam process.

Unfortunately, cast components are susceptible to flaws that are inherent to the casting processes. Although the causes of the flaws are often a function of the type of material being cast, shrinkage pores are common to most if not all materials. In this study, three materials common to the automotive industry were examined: gray cast iron, nodular cast iron and an aluminum-silicon alloy. Regardless of the flaw origin however, if the size is greater than the microstructural

discontinuities of the material (such as flakes, nodules, etc.), the effect is usually a decreased component life.

Cast Iron

The morphology of the graphite in cast iron greatly influences the mechanical properties. The shape, amount and distribution of graphite and its interaction with the matrix largely determine the performance of cast irons under most stress conditions [6]. Past research has studied fatigue considering primarily the initiation and growth of a fatigue crack from a graphite flake or nodule. Gilbert [7] has shown that in nodular cast iron under tensile load, graphite nodules located at the surface can separate from the matrix at the graphite/matrix interface boundary or at the primary/secondary graphite interface. Mitchell [8] has shown that under such circumstances, the nodules can act as spherical voids at which fatigue cracks initiate. The effect of the graphite nodules on fatigue life can also be found in the work of Starkey and Irving [9]. Research done by Ikawa and Ohira [10] have compared the properties of iron with different graphite morphologies and determined that gray cast irons with sharp ended graphite flakes had inferior fatigue properties to nodular in which the nodules posses a lesser stress concentration. Increased graphite flake size results in an increase in notch severity and therefore a decrease in the fatigue resistance [10,11]. The effect of graphite flakes in gray cast iron was studied by many other researchers [11-13] most of whom noted that the susceptibility of a graphite flake to initiating a fatigue crack at low to medium loads was directly related to the orientation of the flake with respect to the plane of maximum stress. However, at higher loads cracks were observed by Mitchell to originate randomly as well as normal to the direction af loading.

Investigators [9,14] have found that failure-related cracks can also initiate at other flaws such as microshrinkage cavities, slag inclusions, blowholes, porosity or irregularly shaped graphite clusters. If such a failure occurred, it was seen that the flaw was more sever than the graphite flake or nodule. This "weakest-link" process is not surprising due to the irregular shape and large size of these casting discontinuities which increase the stress concentration. Regardless of the process, the initiation of a crack in both gray and nodular cast iron has been shown to occur very early in the fatigue life indicating that a crack initiation model alone will not adequately describe the behavior of these materials [9,11,12,15].

Starkey and Irving [16] approximated casting defects found in nodular cast iron to be small cracks and then calculated fatigue lives for a variety of starting defect shapes and sizes. They found that in their specimens, fatigue life is predominantly controlled by pores (because of their larger size and more rapid crack initiation) rather than by nodules and that the variation in observed fatigue lives can be related to the variation in pore size within the iron. Using elastic-plastic fracture mechanics, Starkey and Irving predicted fatigue lives within a factor of four of the

observed lives. Of further interest in their studies is that small pores have initiated failure cracks in preference to nodules larger than themselves suggesting that cracks initiate more readily from the pores. Starkey and Irving [17] later compared the fatigue strength of machined and as-cast surfaces of nodular cast iron and found the as-cast surface to considerably reduce the fatigue life. The studies of Starkey and Irving in general found that to obtain maximum fatigue resistance, the size and number of microshrinkage pores must be kept to a minimum and that the size of the graphite nodules is unimportant.

Aluminum Alloy

Unlike cast iron, fatigue research on aluminum castings is predominantly concerned with the effect of porosity on the fatigue life. Without the presence of microstructural discontinuities similar to the graphite in cast iron, the "weakest-link" in aluminum castings is almost always shrinkage porosity. Suzuki, H. et al [18,19] found that due to a larger amount of porous defects, aluminum casting alloys in general experience a greater amount of scatter in fatigue strength than does cast iron. Couper and Griffiths [20] showed that the S-N properties of an Al-7Si-0.4Mg casting alloy are remarkably insensitive to heat-treatment (either solution treatment or ageing) in contrast to wrought alloys where fatigue resistance is usually closely related to the yield stress or the tensile stress. The difference was accounted for through the observation that fatigue crack initiation occurs at casting defects which were primarily shrinkage pores. An additional observation of Couper and Griffiths was that reducing the size of shrinkage defects will increase the fatigue life, but only up to the stage at which initiation from persistent slip bands on the surface becomes operative. In order to take into account the initiating flaw, Couper and Griffiths modified an S-N diagram by plotting the stress amplitude versus the product of the initial flaw depth and the specimens corresponding fatigue life. They found this technique to substantially reduce the observed scatter in fatigue life.

Suzuki and Kunio [21] performed rotating fatigue tests on two types of Al-Si-Cu aluminum casting alloys having different solid solution heat treatments. They found that the difference in fatigue life between the different heat treated materials resulted from a difference in porosity size and distribution. They found that a relationship of $S\sqrt{\pi d}$ and log N has a greater degree of correlation than does plotting stress amplitude versus cycles-to-failure alone, where d is the size of the porous defect.

Scope of Study

The effect of porosity on the fatigue and monotonic properties of three cast materials used widely in the automotive industry was examined. Fatigue tests were carried out on the three materials after which the initiating flaw sizes were examined and measured. As an aid to

automotive component design, a method of fatigue life prediction based on Linear Elastic Fracture Mechanics was developed and tested in order to account more accurately for the influence of porosity. The calculated predicted lives were then compared to the actual lives.

2. EXPERIMENTAL PROCEDURES

2.1 Material Description and Geometry

Cast Iron: Specimens of nodular and gray cast iron were cast by the General Motors Corporation using the lost-foam and the empty-cavity casting methods. The specimens for each process considered were cast from the same heat. A chemical analysis was performed on the materials by Chicago Spectro Service Laboratory, Inc., and the results are presented in Table 1. Micrographs of the nodular cast iron for the two casting processes are shown in Figs. 1-2. The material is a pearlitic nodular cast iron with graphite nodules encased in a ferritic shell separated by grains of pearlite. The lost-foam process resulted in smaller grains than did the empty-cavity process. This difference in the grain size affected the monotonic properties as will be discussed later. Shown in Figs. 3-4 are the microstructures of the gray cast iron . The matrix consists of both pearlite and ferrite with a slightly greater amount of ferrite than is present in the G-LF material. Tensile tests of machined specimens were performed using a 20 kip MTS servo-hydraulic testing machine at a strain rate of 0.0005 sec^{-1}. Brinell hardness tests were carried-out on the nodular cast iron using a 10mm diameter steel ball indenter with a 3000 kg load applied for 15 seconds. The gray cast iron fractured under the applied 3000 kg load so a load of 1500 kg was used. Table 2 contains the results of the monotonic testing.

The specimens cast using the empty-cavity method were machined to the dimensions shown in Fig. 6, and the gage-sections were polished to a 12μm surface finish. The specimens that were cast using the lost-foam method were divided into two groups; one of which was machined as described above and the other tested with the as-cast surface. A summary of the specimen types and the specimen numbering code:

- Nodular cast iron cast using the empty-cavity method tested with a surface finish of 12μm (N-EC-#).
- Nodular cast iron cast using the lost-foam method tested with a surface finish of 12μm (N-LF-#).
- Nodular cast iron cast using the lost-foam method tested with the surface in the as-cast condition.(N-LF-#ac).
- Gray cast iron cast using the empty-cavity method tested with a surface finish of 12μm (G-EC-#).
- Gray cast iron cast using the lost-foam method tested with a surface finish of 12μm (G-LF-#).
- Gray cast iron cast using the lost-foam method tested with the surface in the as-cast condition.(G-LF-#ac).

In the early stages of the test program, an x-ray examination was performed on each specimen before it was tested. However, the resolution of the radiographs was so poor that no defects could be seen, and examination of this type in the test program was stopped.

Aluminum-Silicon Alloy: Specimens of AlSi 319 aluminum alloy were cast by the General Motors Corporation using the lost-foam process and T5 heat-treated. The specimens were received as 0.625 in. diameter, 12 in. long bars. Specimens were machined to the final dimensions shown in Fig. 7. As-cast-gage-section samples were received ready to test and only the grip ends required any further machining. A chemical analysis was performed on the material by Chicago Spectro Service Laboratory, Inc., and the results are presented in Table 2. A micrograph of the AlSi alloy, exhibiting the distribution of silicon in the matrix, is shown in Fig. 5. Brinell hardness tests using a 10mm diameter steel ball with a 500 kg load and tensile tests were performed in the same manner as the cast iron described above. The results of the monotonic tests are presented in Table 3.

2.2 Fatigue Tests

Room temperature, load-controlled fatigue tests were performed using a 20 kip MTS servo-hydraulic testing machine. The load ratio was R = 0.1 and the test frequency was f = 10 Hz. Failure was defined as complete separation of the specimen. If the specimen did not fail by 10 million cycles (10^7), the test was stopped; and the result was labeled as "runout". The aluminum-silicon alloy was tested under two different environments: a room temperature, 99% relative humidity environment achieved using a Tygon tube through which water-saturated air was circulated and a 300 °F, laboratory air environment achieved using a Thermolyne heat tape which was wrapped around the gage section of the specimen. These tests were also carried-out at R = 0.1 and f = 10 Hz. Scanning electron microscope (SEM) examination of the fracture surfaces was performed on all specimens to determine the existence, location, type and size of an initiating flaw. Macrophotos were taken on selected specimens to determine an average crack aspect ratio.

2.3 Surface Crack-Growth Observation

The surface of selected specimens was replicated to monitor crack development using the following procedure: Clear acetyl cellulose film (0.034mm thick) was softened with a methyl acetate solution (Kodak 520) and placed on the gage-section of the specimen. Once dry, the film was stripped and viewed using a light microscope. The length of a crack on the surface was measured and related to the depth of the crack using an assumed constant aspect ratio [22].

A summary of the testing procedure is presented as block-diagrams in Figs. 8 and 9.

3. RESULTS AND DISCUSSION

3.1 Observed Flaw Geometry

The geometry of the initiating flaws can be divided into three categories: A semi-elliptical surface flaw (Type I) which was by far the most common shape; an internal circular flaw (Type II); and a long, cylindrical flaw originating at the surface (Type III). Fractographs of examples of the three flaw types are presented in Figs. 10-12. The initiating flaws found in the AlSi alloy were all categorized as Type I, semi-elliptical flaws. An example of a shrinkage cavity in the AlSi alloy at which a fatigue crack initiated is shown in Fig. 13.

3.2 Fatigue Test Results

Nodular Cast Iron : The results of the nodular cast iron fatigue tests are listed in Tables 4 and 5. The corresponding stress-life diagram (S-N diagram) is found in Fig. 16. While the maximum stress alone plays an important role in the fatigue life of these specimens, it is not the only parameter that should be considered. The initiation-flaw type, flaw size, and flaw location are also important. Therefore the initial stress intensity factor, ΔK_0, was used as a parameter to correlate the observed fatigue lives.

Post failure measurements of the fracture surface indicate the final flaw to be semi-elliptical in shape (Fig. 21) with an average aspect ratio (a/c) of 0.913. Therefore, a semi-elliptical surface flaw model was used for a Type I flaw: see Fig. 29 and Appendix A. In Fig. 29 it is shown that in the determination of ΔK_0, an equivalent rectangular cross-section was assumed based on the cross-section of the round-bar specimen . The depth of the flaw was measured to determine a_0 from which the shape of the semi-ellipse was determined based on the assumed aspect ratio of a/c = 0.913. To determine the initial stress intensity factor (ΔK_0) of a Type II flaw, an embedded circular slit-crack model was implemented as described in Appendix A. Past research [22] has shown that approximating a small (< 0.5 mm) Type III flaw as a semi-ellipse is appropriate, and this practice was continued in this study.

Table 10 lists the initial ΔK_0 values of the empty-cavity nodular cast iron. Figure 19 shows a plot of ΔK_0 (calculated with the initial flaw depth) versus cycles to failure for the empty-cavity nodular cast iron specimens. Figure 19 indicates a good correlation between the values of ΔK_0 and N_f. A comparison of the S-N diagram and the ΔK_0-N diagram for this material shows that the coefficient of correlation based on a best-fit logarithmic line increases from r = 0.20 and r = 0.88.

Table 11 gives the initial ΔK_0 values of the lost-foam nodular cast iron. Figure 19 also demonstrates the dependance of N_f on the initial stress intensity factor of the initiating flaw for the lost-foam nodular cast iron. The coefficient of correlation in this case increases from r = 0.50 to r = 0.91.

Gray Cast Iron: The results of the gray cast iron fatigue tests are listed in Tables 6 and 7. The stress versus cycles-to-failure curve is found in Fig. 17. Figure 14 shows a large flaw on the surface of specimen G-LF-15 before testing. Figure 15 on the same page is a macrograph of the fracture surface after fatigue testing at 75.8 MPa (N_f = 120,000 cycles) in which it is clear that their is no distinguishable casting flaw on the surface. Further examination using an electron microscope gave no information as to an exact location of fatigue crack initiation. This type of behavior was very common (only 10% of the specimens tested failed at a casting-flaw compared to 100% for the nodular) and can be attributed to the nature of the carbon flakes in the microstructure - each one acting as small, sharp cracks that eventually link up as the fatigue cycles progress resulting in a sudden, fast-fracture [13]. The average (mean) size of a_0 for the gray cast iron was 2.87 mm compared with 0.72 mm for the nodular cast iron This difference suggests that the carbon flakes in the microstructure control the fatigue life unless a flaw with a larger stress concentration is present. The fatigue life of gray cast iron, in general, showed a much better correlation to the applied stress than did the nodular cast iron.

Table 12 lists the initial ΔK_0 values of the empty-cavity and lost-foam gray cast iron. Figure 19 shows a plot of ΔK_0 (for those specimens that failed from a casting defect) versus cycles to failure for the G-EC and G-LF cast iron specimens. The data show a good correlation between the initial stress intensity factor of a large casting flaw and the specimen's corresponding fatigue life.

Unlike the empty-cavity gray cast iron, the lost-foam gray cast iron had considerable surface porosity. Although the G-EC material showed slightly better fatigue properties than G-LF, examination of the fracture surface gave no apparent indication that the surface porosity was responsible for the difference.

Aluminum-Silicon: The results of the aluminum fatigue tests are listed in Tables 8-9. The corresponding stress versus cycles-to-failure curve is found in Fig. 18. Test temperatures and surface finish had no significant effect on the fatigue strength of this alloy. Rather, as will be shown, the scatter in the test results was determined by the size of the largest casting pore.

Table 13 lists the initial ΔK_0 values of the AlSi-319 alloy. The values of the stress intensity factor were calculated using the semi-elliptical surface model described above and in Fig. 29. The aspect ratio (a/c) for the AlSi was calculated to be approximately 0.950. Figure 20 shows a plot of ΔK_0 versus cycles-to-failure for the specimens tested at room temperature at 99% humidity and 300°F. Figure 20 shows that a very good relationship exists between ΔK_0 and the fatigue life.

Some failures initiated in the grip-end sections of the specimens, where the stresses were nominally 36% of the stresses in the gage section. It is questionable whether the stresses in these grip section locations are accurately known since many of the gage section initiation sites are within

one diameter of the grips and the large surface shear stresses applied by the grips. The grip section data are therefore distinguished from the gage section failures by being plotted as solid symbols in Fig. 18, and the low values for these data are suspect.

These grip section failures indicate that fatigue cracks do not necessarily originate in the regions of the highest nominal stresses, but often in lower stress locations were the largest defect is located. More exactly, fatigue failure should initiate at the location having the highest initial value of stress intensity factor.

3.3 Measurement of Crack Growth Rates

Nodular Cast Iron: Fatigue cracks of the nodular cast iron specimens could always be traced back to their initiation site through an examination of the fracture surface. As shown in Fig. 21, the crack began at a small flaw, grew in a semi-elliptical manner, and finally caused fracture. In general, the initiating flaws were notches that resulted from the casting processes; and, with few exceptions, they were located at the surface of the specimen. The cracks propagated in a direction perpendicular to the maximum principal stress (Forsyth Stage II cracks [7]). The replication studies indicated that the cracks initiated within the first 10% of the total fatigue life. Thus, the majority of the fatigue life was spent in crack growth.

Fatigue crack growth rate was measured through examination of the surface replicas. An attempt was made to obtain crack-length data for long-life fatigue (>100,000 cycles); but due to the dependence of the fatigue life on the initial flaw size and location, the specimens failed short of this goal in some cases. The analysis was nevertheless performed using the LEFM model that will be described in a later section.

A plot of crack length versus completed cycles for empty cavity nodular cast iron is shown in Fig. 23. From this plot, the crack-growth rate was calculated using the seven-point polynomial method: see Appendix C. Values of da/dN were then plotted versus ΔK_I (Fig. 32) and the characteristic linear region extrapolated to the Y-intercept. A logarithmic best-fit line indicates the Paris power law constants to be : $C \approx 1.02 \times 10^{-20}$ meters/cycle and $m \approx 8.98$. Although these values are extreme when compared to past research performed on similar materials using strain-controlled tests [6], the results of the life prediction (discussed in Section 3.5) using these constants were quite reasonable. Similarly, a plot of crack length versus completed cycles for lost-foam cast iron is shown in Fig.24. Because of a limited number of data points, the seven-point polynomial method could not be used (this method requires at least seven points to calculate one value of da/dN). In these cases, an averaging exponential best-fit was applied to the data after which the crack growth rate could be determined mathematically: see Fig. 24. This method has been used successfully in the past [22] on brittle materials and produces similar results in the linear region of log da/dN versus log N as does the seven-point polynomial method.

A plot of da/dN versus ΔK for the lost-foam cast iron (with an extended linear region) is found in Fig. 27. The Paris power law constants were determined to be: $C \approx 5.25 \times 10^{-14}$ meters/cycle, $m \approx 3.99$ for specimen N-LF-8 and $C \approx 5.85 \times 10^{-14}$ meters/cycle, $m \approx 3.67$ for specimen N-LF-13. An average of these values was used in the life prediction.

Gray Cast Iron : The replication of the gray cast iron was carried out in a manner similar to the nodular cast iron. However, due to the nature of the microstructure of the material, it was very difficult to predict the location of crack initiation; and in many cases, the specimen either failed in the grip section, failed out of the zone of replication, or no dominant crack could be located. Consequently, only one specimen (G-EC-18) provided useful crack growth data.

Figure 26 is a plot of crack length versus completed cycles of specimen G-EC-18. The crack initiated at and grew from a semi-elliptical flaw located at the surface. Crack growth was observed after 10% of the total life thereby indicating the dominance of propagation. The plot of da/dN versus ΔK is found in Fig. 28. Although the fracture surface did not imply that the crack grew in any particular shape (see Fig. 30 for example), it was assumed, based on post-failure fractography, that the crack grew as a semi-ellipse in a manner similar to the nodular cast iron tested in this program. The results of the test give the Paris power law constants: $C \approx 2.98 \times 10^{-11}$ meters/cycle and $m \approx 3.71$.

The fatigue data obtained from the testing of the gray cast iron specimens containing casting flaws is very limited. Without knowing the distribution of flaws throughout the specimens, it could not be concluded whether or not the casting flaws played a significant role in the fatigue life of the gray cast iron, and if so to what degree.

Aluminum-Silicon: Fatigue cracks in the machined-surface specimens could be traced back to their initiation site which usually was at the edge of a shrinkage cavity on the specimen surface. The same was generally true for the as-cast specimens, but in two cases the fatigue crack initiated as a result of the surface roughness which provided the critical notch.

Siljander [22] performed replication studies on the Aluminum-Silicon 319 material using an averaging exponential best-fit line similar to the method performed on the lost-foam nodular cast iron and the gray cast iron described above. The Paris Power Law Constants were conservatively estimated to be $C \approx 2.05 \times 10^{-10}$ meters/cycle and $m \approx 3.12$.

3.4 Fatigue Life Predictions Based on Linear Elastic Fracture Mechanics

Because the replication tests indicated that the fatigue cracks growing from a casting flaw is primarily dominated by crack-propagation, the Paris power law was used to predict the fatigue lives of the specimens:

$$\frac{da}{dN} = C(\Delta K)^m$$

where: ΔK is the mode I stress intensity factor.

Integration of this equation leads to the following expression :

$$N_P = \frac{1}{C}\int_{a_0}^{a_f} (\Delta K)^{-m} da$$

From which the fatigue life can be calculated in one of two manners : (1) a numerical integration can be employed, with the use of a computer, based on the following equation :

$$da = C\,(\Delta K)^m\, dN$$

In this method the crack length is calculated on a cycle-to-cycle basis from the measured initial flaw size to an assumed final flaw size based on fracture mechanics. When the value of crack length, a, reaches the final length or when the value of K_{max} reaches a chosen K_Q, the number of calculations performed (if dN is chosen to be 1) is equal to the predicted propagation life. (2) The Mode I geometry correction factor for the semi-elliptical flaw, Y_1, has been shown [23] to be almost constant (0.71) for aspect ratios of 0.5 to 1.0. The fatigue life can therefore be estimated using the following expression :

$$N_P = \frac{a_f^{1-(m/2)} - a_0^{1-(m/2)}}{C\left(0.913\, Y_1 \Delta\sigma\sqrt{\pi}\right)} \frac{1}{1-\frac{m}{2}}$$

where N_P is the predicted propagation life.

In either case, the predicted life is most dependent upon the initial flaw size while the influence of final flaw size is much less significant. In this study, the first method of life prediction was used on the cast iron (in order to account more accurately for variances in the specimen diameter) using $K_Q = 47.7$ MPa(m)$^{0.5}$ determined from post-failure SEM measurements. The second method was used on the AlSi-319 alloy. The final flaw size was calculated using the value of plane-strain fracture toughness, $K_Q = 16.5$ MPa(m)$^{0.5}$ found in reference 22. The fatigue life predictions are included in Tables 10, 11 and 13. Gray cast iron predictions were not performed due to the dependance of fatigue life on the graphite flakes and not the porosity.

3.5 Comparison of Predicted and Observed Fatigue Lives

Cast Iron: The actual fatigue test results of the empty-cavity nodular cast iron are compared with the analytical fatigue life predictions in Table 10. The prediction is based on the post-failure

SEM measurements of the initiating flaw. The flaws were measured along the fracture surface to the deepest portion (into the specimen) to determine a_0. The shape of the initial flaw was then approximated as a semi-elliptical shape, assuming a constant aspect ratio of a/c = 0.913 in the manner shown in Fig. 29. A plot of the predicted lives versus the actual lives of empty-cavity nodular cast iron are shown in Fig. 30 which indicates that the majority of observed lives agree with the predicted lives within a factor of two. The predictions become more conservative (under-prediction) at long lives.

A comparison of the actual fatigue test results and the fatigue life predictions of lost-foam nodular cast iron is contained in Table 11. The predictions are based on SEM flaw measurements in the manner described above. A plot of the predictions versus the actual lives is found in Fig. 30. The majority of lives in this case also agree within a factor of two, and the predictions become more conservative at longer lives. Figure 32 contains a curve of the predicted lives over-laying a plot of ΔK_0 versus cycles to failure for the nodular cast iron. The actual lives agree quite well with the predictions but become increasingly conservative at longer lives. This trend suggests a need to consider an initiation model in addition to the propagation model used in this study.

Aluminum-Silicon 319: The actual fatigue tests results and the analytical fatigue life predictions of the AlSi-319 alloy are listed in Table 13. The predictions are based on SEM flaw measurements and approximating the defects as semi-elliptical flaws as was described above. The actual versus predicted fatigue life results in Table 13 are displayed graphically in Fig. 31. Most of the predicted lives agree with the actual lives within a factor of two.

The crack growth constants C and m in the Paris expression were not determined according to the ASTM standard (E 647) but were determined using a load ratio of R = 0.1 with the specimen geometry described in Fig. 3. Actual service history measurements by General Motors have shown the value of R to be closer to 0.9 [1]. Figure 33 contains a curve of the predicted lives over-laying a plot of ΔK_0 versus cycles to failure for the AlSi-319 alloy. The graph in this case suggests that the propagation model is useful at long and short lives and that initiation need not be considered.

3.6 Suggestions for Future Work

The life prediction model implemented in this study was based solely on the dominance of crack propagation during the fatigue life of the specimen. The cast iron life predictions become increasingly conservative suggesting that while a crack propagation model is appropriate at short lives ($<10^6$ cycles), at long lives the importance of crack initiation should be considered. The aluminum-silicon fatigue life predictions on the other hand suggest that a crack propagation model

is applicable at both long and short lives. The importance of fatigue initiation at long fatigue lives for the aluminum-silicon should be further investigated.

A detailed study of the threshold stress intensity and plain-strain fracture toughness is suggested to determine design limits on the size of acceptable porosity for a given component. These tests may be performed by directly casting compact tension specimens to evaluate ΔK_{th} and K_{IC}.

In this study, the existence of residual stresses was not considered. Mean stress effects resulting from residual stresses should be examined in future work.

Finally, it should be noted that components in service seldom experience stress histories that are constant amplitude. A program of variable amplitude fatigue testing could be considered.

4. CONCLUSIONS

4.1 Nodular Cast Iron

1. Every nodular cast iron specimen failed as a result of a crack that initiated at and grew from a casting-flaw. Casting-flaws played a major role in the fatigue behavior of both empty-cavity and lost-foam nodular cast iron.
2. Specimens containing flaws that were located internally beyond a pore diameter of the surface had an appreciably longer fatigue life.
3. The lost-foam nodular cast iron had slightly better fatigue properties in the shorter life (<100,000 cycles) regime than did the empty-cavity nodular cast iron. However, in the long-life regime, the data suggests that lost-foam nodular cast iron has slightly worse fatigue properties.
4. There is a better correlation between the initial stress intensity factor of the initiating flaw and the fatigue life than with the maximum stress (R = 0.1).
5. A fatigue crack growth model, which treated the surface flaws as semi-elliptical surface flaws in tension, was used to predict the fatigue lives of the nodular cast iron within a factor of two. The predictions were increasingly conservative (under-prediction) at long lives.

4.2 Gray Cast Iron

1. Only a small number of gray cast iron specimens failed as a result of fatigue cracks that initiated at a casting flaw.
2. There is a better relationship in the gray cast iron between the maximum stress (R = 0.1) and the fatigue life than was observed for the nodular cast iron tests.
3. The lost-foam gray cast iron contained a considerable amount of surface porosity.
4. The lost-foam gray cast iron in general had shorter fatigue lives than did the empty-cavity cast iron.

4.3 Aluminum-Silicon 319

1. The surface finish of the samples had only a small effect on the fatigue characteristics of the AlSi 319 alloy.
2. The testing temperature had only a small effect in the fatigue behavior of the AlSi 319 alloy.

3. The shrinkage cavities played a major role in the fatigue behavior of the lost-foam AlSi 319 alloy. These defects were due to the casting process, and they provided very irregular near-surface flaws.
4. The fatigue cracks initiated either from the multiple casting pores, from the surface texture triple points, or from the combination of the two. These flaws then grew perpendicular to the fluctuating tensile principal stress. The majority of the fatigue life was spent propagating fatigue cracks. The location of the largest pore always dictated the fatigue crack initiation site.
5. A fatigue crack growth model, which treated the surface flaws as semi-elliptical surface flaws in tension, was used to predict the fatigue lives of the aluminum-silicon 319 alloy within a factor of two.

5. REFERENCES

1. Kanicki, D. P.; 'Casting Advantages, Applications, and Market Size', Metals Handbook, Ninth Edition, Volume 15, ASM International, Metals Park, Ohio, pp. 37-45.

2. 'Competitive Assessment of the U.S. Foundry Industry', USITC Publication 1582, U.S. Department of Commerce, Sept 1984, p. xiii.

3. Sikora, E. J.; 'Evaporative Casting Using Expendable Polystyrene Patterns and Unbonded Sand Casting Techniques', Transactions of the American Foudrymen Society, Volume 86, American Foundrymen Society, DesPlaines, Illinois, 1978, p. 65.

4. Ashton, M. C., Sharman, S. G., Brookes, A. J.; 'The Replicast (Full Mold) and CS (Ceramic Shell Process)', Transactions of the American Foudrymen Society, American Foundrymen Society, DesPlaines, Illinois, Volume 92, pp. 271-280.

5. Patz, M., Piwonka, T. S.; 'Unbonded Sand Molds', Metals Handbook, Ninth Edition, Volume 15, ASM International, Metals Park, Ohio, pp. 230-237.

6. Hua, C. T.; 'Fatigue Crack Growth in Nodular Cast Iron', FCP Report No. 47. College of Engineering, University of Illinois at Urbana-Champaign, Urbana, IL (1983).

7. Gilbert, G. N. J.; 'The Stress/Strain Properties of Nodular Cast Iron in Tension and Compression', J. BCIRA, Volume 3 (1967), pp. 11-21.

8. Mitchell, M. R.; 'A Unified Predictive Technique for the Fatigue Resistance of Cast-Ferrous Based Metals and High Hardness Wrought Steels', FCP Report No. 23, College of Engineering, University of Illinois at Urbana-Champaign, Urbana, IL (1976).

9. Starkey, M. S., Irving, P. E.; 'The Influence of Microstructure on Fatigue Crack Initiation in Spheroidal Graphite Cast Iron', GKN Technical Report, GKN Group Technological Centre, Wolverhampton, England (1979).

10. Ikawa, K., Ohira, G.; 'Fatigue Properties of Cast Iron in Relation to Graphite Structure', Journal of Cast Metals Research, Volume 12, No. 2 (1964), pp. 170-193.

11. Mitchell, M. R.; 'The Effect of Graphite Morphology, Matrix Hardness and Structure on the Fatigue Resistance of Gray Cast Iron', Society of Automotive Engineers, Report No. 750198, (1975).

12. Fash, J. W.; 'Fatigue Crack Initiation and Growth in Gray Cast Iron', FCP Report No. 35. College of Engineering, University of Illinois at Urbana-Champaign, Urbana, IL (1980).

13. Socie, D. F., Fash, J. W., Downing, S. D.; 'Fatigue of Gray Iron', FCP Report No. 44, College of Engineering, University of Illinois at Urbana-Champaign, Urbana, IL (1982).

14. Testin, R. A.; 'Characterization of the Cyclic Deformation and Fracture Behavior of Nodular Cast Iron', Department of Theoretical and Applied Mechanics, Report No. 371, College of Engineering, University of Illinois at Urbana-Champaign, Urbana, IL (1973).

15. Biell, A. J., Lawrence, F.V., 'The Mechanical Properties of Lost-Foam Nodular and Gray Cast Iron - The Effect of Casting Porosity', Report to the General Motors Corporation, College of Engineering, University of Illinois at Urbana-Champaign, Urbana, IL (1989).

16. Starkey, M. S., Irving, P. E.; 'Prediction of Fatigue Life of Smooth Specimens of SG Iron by Using a Fracture Mechanics Approach', Proc. of Int. Symp. on Low-Cycle Fatigue and Life Prediction, Firminy, France, 1980: ASTM Publication PCN 04-770000-30, pp. 382-398.

17. Starkey, M. S., Irving, P. E.; 'A Comparison of the Fatigue Strength of Machined and As-Cast Surfaces of SG Iron', International Journal of Fatigue, Volume 4, No. 3, (1982), pp. 129-136.

18. Suzuki, H. et al; 'Roll of Microstructure and Mechanical Properties on Fatigue Strength of Vermicular and Nodular Iron', Trans. of JSME, 50-451, A (1984), p. 520.

19. Suzuki, H. et al; 'Influence of Matrix Structure on Fatigue Strength of Nodular Iron with High Tensile Strength', Trans. of JSME, 51-464, A (1985), p. 1225.

20. Couper, M. J., Griffiths, J. R.; 'Casting Defects and the S-N Fatigue Behaviour of an Aluminum Casting Alloy', Proc. of the 1985 Symposium of the Australian Fracture Group, Sydney, N. S. W., Australia, University of Sydney (1985), pp. 75-84.

21. Suzuki, H., Kunio, T.; 'Influences of Porous Defect on Scatter of Fatigue Strength of Aluminum Casting Alloy, AC4B (JIS)', Proc. of the Role of Fracture in Modern Technology Conference, Fukuoka, Japan, 1986: Elsevier Science Publishers B.V., Amsterdam, The Netherlands (1987), pp. 225-232.

22. Siljander, A., Lawrence, F.V.: 'The Mechanical Properties of Al-Si 319, The Role of Casting Porosity'. Report to the General Motors Corporation. College of Engineering, University of Illinois at Urbana-Champaign, Urbana, IL (1988).

23. Ewalds, H. L., Wanhill, R. J. H.: Fracture Mechanics. Delftse Uitgevers Maatschappij, Delft, The Netherlands (1986).

24. Hua, C. T.: 'Fatigue Damage and Small Crack Growth During Biaxial Loading'. Report No. 109. Department of Mechanical and Industrial Engineering, University of Illinois at Urbana-Champaign, Urbana, IL (1984).

25. Weinacht, D. J.: 'Fatigue Behavior of Gray Cast Iron Under Torsional Loads'. Report No. 126. Department of Mechanical and Industrial Engineering, University of Illinois at Urbana-Champaign, Urbana, IL (1986).

26. Forsyth, P. J. E.:'A Two-Stage Process of Fatigue Growth.' Proc., Crack Propagation Symposium, Cranfield (1961), pp 76-94.

27. ASTM E602-81. 'Standard method for Sharp-Notch Tension Testing With Cylindrical Specimens'. American Society for Testing and Materials, 1981.

28. Fuchs, H. O., Stephens, R. I.: Metal Fatigue in Engineering. John Wiley & Sons; Toronto, Canada (1980).

29. Brick, R. M., Pense, A. W., Gordon, R. B. : Structure and Properties of Engineering Materials. McGraw-Hill Book Company; New York, New York (1977).

TABLE 1

CHEMICAL COMPOSITIONS OF THE NODULAR AND GRAY CAST IRONS IN WEIGHT PERCENT *

Element	Nodular Empty Cavity (N-EC)	Nodular Lost Foam (N-LF)	Gray Empty Cavity (G-EC)	Gray Lost Foam (G-LF)
Carbon	3.79 %	3.62 %	3.66 %	3.76 %
Silicon	2.55	2.55	2.70	2.72
Manganese	0.63	0.83	0.81	0.71
Copper	0.16	0.13	0.30	0.36
Chromium	0.03	0.06	0.34	0.26
Magnesium	0.030	0.024	<0.005	<0.005
Phosphorus	0.024	0.024	0.037	0.018
Nickel	0.01	0.07	0.01	0.08
Molybdenum	<0.01	<0.01	<0.01	<0.01
Sulfur	<0.005	0.008	0.022	0.014

TABLE 2

CHEMICAL COMPOSITIONS OF THE ALUMINUM-SILICON 319 ALLOY IN WEIGHT PERCENT *

Si	Cu	Mg	Fe	Ti	Zn	Mn	Pb	Sn	Ni	Cr
5.70	3.04	0.75	0.20	0.08	<0.05	<0.05	<0.05	<0.05	<0.05	<0.05

* The data were supplied by Chicago Spectro Service Laboratory, Inc.
4848 S. Kedzie Ave., Chicago, Il 60632 (312) 523-7088

TABLE 3

MONOTONIC PROPERTIES OF THE CAST IRON AND ALUMINUM SILICON ALLOY IN LABORATORY AIR

	Nodular Empty Cavity (N-EC)	Nodular Lost Foam (N-LF)	Gray Empty Cavity (G-EC)	Gray Lost Foam (G-LF)	Al-Si Lost Foam
Ultimate Tensile Strength (MPa)	605	747	185	156	228.1
0.2% - Offset Yield Strength (MPa)	387	509	145	141	228.1
Percent Reduction in Area (%)	11.2	6.37	0.31	0.59	0.26
Elastic Modulus (GPa)	164	178	61	52	*
Brinell Hardness (BHN)	220[1]	265[1]	166[2]	156[2]	52.0[3]

[1] 10 mm ball @ 3000 Kg load

[2] 10 mm ball @ 1500 Kg load

[3] 10 mm ball @ 500 Kg load

* The information is unavailable

TABLE 4

FATIGUE TEST RESULTS OF EMPTY-CAVITY NODULAR CAST IRON

Specimen I.D.	Maximum Stress MPa	ksi	Cycles to Failure	Flaw Type	Initial Flaw Depth, a_0 (mm)
N-EC-5	324.1	47.0	>10,000,000	†	†
N-EC-37	337.9	49.0	>10,000,000	†	†
N-EC-2	344.8	50.0	>10,000,000	†	†
N-EC-4	344.8	50.0	363,500	I	0.200
N-EC-23	348.2	50.5	44,300	I	0.929
N-EC-11	349.6	50.7	31,500	I	1.333
N-EC-16	351.6	51.0	>10,000,000	†	†
N-EC-9	355.1	51.5	2,039,400	II	0.417
N-EC-13	355.1	51.5	17,000	I	5.700
N-EC-25	358.5	52.0	144,300	I	0.610
N-EC-3	362.0	52.5	339,500	I	0.241
N-EC-18	365.4	53.0	977,300	I	0.320
N-EC-26	368.9	53.5	302,300	I	0.267
N-EC-36	368.9	53.5	185,700	I	0.240
N-EC-38	368.9	53.5	159,000	I	0.530
N-EC-20	372.3	54.0	675,700	I	0.140
N-EC-24	375.8	54.5	210,000	I	0.260
N-EC-31	375.8	54.5	251,900	III	0.300
N-EC-7	379.2	55.0	6,213,400	II	0.165
N-EC-29	382.7	55.5	1,105,500	I	0.074
N-EC-6	386.1	56.0	>10,000,000	†	†
N-EC-1	393.0	57.0	48,200	I	0.420
N-EC-8	413.7	60.0	219,200	I	0.120

† Not Applicable

Flaw Type:

I Semi elliptical flaw originating at the surface
II Embedded internal circular flaw
III Long, cylindrical flaw originating at the surface

R = 0.1
f = 10 Hz

TABLE 5

FATIGUE TEST RESULTS OF LOST-FOAM NODULAR CAST IRON

Specimen I.D.	Maximum Stress MPa	ksi	Cycles to Failure	Flaw Type	Initial Flaw Depth, a_o (mm)
N-LF-5	275.8	40.0	>10,000,000	†	†
N-LF-26	310.3	45.0	37,400	I	2.267
N-LF-36	310.3	45.0	>10,000,000	†	†
N-LF-38	310.3	45.0	336,120	II	0.960
N-LF-40	310.3	45.0	>10,000,000	†	†
N-LF-39	331.0	48.0	335,600	I	0.257
N-LF-1	344.8	50.0	>10,000,000	†	†
N-LF-6	344.8	50.0	328,300	III	0.470
N-LF-23	344.8	50.0	666,700	I	1.044
N-LF-24	344.8	50.0	>10,000,000	†	†
N-LF-11	365.4	53.0	366,700	I	0.311
N-LF-30	372.3	54.0	59,700	III	0.899
N-LF-10	379.2	55.0	681,900	I	0.250
N-LF-18	379.2	55.0	295,100	I	0.429
N-LF-21	379.2	55.0	305,900	I	0.210
N-LF-29	389.6	56.5	22,500	I	1.834
N-LF-2	413.7	60.0	101,600	I	0.333
N-LF-13	413.7	60.0	85,400	I	0.846
N-LF-20	448.2	65.0	134,500	I	0.225
N-LF-3	482.7	70.0	25,400	I	0.513
N-LF-8	482.7	70.0	46,000	I	0.510
N-LF-19	517.1	75.0	52,300	I	0.170
N-LF-25ac	110.3	16.0	>10,000,000	†	†
N-LF-16ac	137.9	20.0	>10,000,000	†	†
N-LF-9ac	197.7	28.7	615,700[1]	I	1.180
N-LF-7ac	241.3	35.0	>10,000,000	†	†
N-LF-4ac	263.8	38.3	2,097,700	I	1.922
N-LF-15ac	328.1	47.6	397,700	I	1.376
N-LF-22ac	330.5	47.9	2,613,400	II	0.889
N-LF-14ac	340.5	49.4	1,312,100	II	0.367
N-LF-12ac	373.3	54.1	469,400	II	0.435
N-LF-17ac	578.4	83.9	5,100	I	0.432

† Not Applicable

Flaw Type:

I Semi elliptical flaw originating at the surface
II Embedded internal circular flaw
III Long, cylindrical flaw originating at the surface

Remarks:

1 Failed in the grip-section

TABLE 6

FATIGUE TEST RESULTS OF EMPTY-CAVITY GRAY CAST IRON

Specimen I.D.	Maximum Stress MPa	ksi	Cycles to Failure	Flaw Type	Initial Flaw Depth, a_o (mm)
G-EC-14	69.0	10.0	>10,000,000	†	†
G-EC-23	82.7	12.0	>10,000,000	†	†
G-EC-1	96.5	14.0	183,000	none	†
G-EC-11	96.5	14.0	>10,000,000	†	†
G-EC-25	96.5	14.0	22,700	III	3.120
G-EC-29	96.5	14.0	>10,000,000	†	†
G-EC-30	96.5	14.0	170,500	III	2.263
G-EC-3	100.0	14.5	590,600	none	†
G-EC-13	100.0	14.5	443,300	none	†
G-EC-18	100.0	14.5	47,900	I	0.749
G-EC-21	100.0	14.5	3,941,700	none	†
G-EC-5	103.4	15.0	>10,000,000	†	†
G-EC-6	103.4	15.0	123,700	none	†
G-EC-9	103.4	15.0	167,200	none	†
G-EC-10	103.4	15.0	24,600	III	1.990
G-EC-19	103.4	15.0	52,400	none	†
G-EC-4	110.3	16.0	36,600	none	†
G-EC-27	110.3	16.0	5,900	I	††
G-EC-15	137.9	20.0	3,800	none	†
G-EC-26	275.8	40.0	0	none	†
G-EC-20	344.8	50.0	0	none	†

† Not Applicable
†† The flaw was of substantial size.

Flaw Type:
I Semi elliptical flaw originating at the surface
III Long, cylindrical flaw originating at the surface

R = 0.1
f = 10 Hz

TABLE 7

FATIGUE TEST RESULTS OF LOST-FOAM GRAY CAST IRON

Specimen I.D.	Maximum Stress MPa	ksi	Cycles to Failure	Flaw Type	Initial Flaw Depth, a_o (mm)
G-LF-14	69.0	10.0	>10,000,000	†	†
G-LF-7	62.1	9.0	>10,000,000	†	†
G-LF-20	64.1	9.3	>10,000,000	†	†
G-LF-1	65.5	9.5	>10,000,000	†	†
G-LF-18	65.5	9.5	>10,000,000	†	†
G-LF-3	69.0	10.0	667,700	none	†
G-LF-17	69.0	10.0	540,200	none	†
G-LF-23	72.4	10.5	252,700	none	†
G-LF-21	74.1	10.8	50,100	none	†
G-LF-19	75.8	11.0	207,000	none	†
G-LF-2	75.8	11.0	1,500	I	5.080
G-LF-15	75.8	11.0	120,800	none	†
G-LF-24	77.6	11.3	79,800	none	†
G-LF-16	79.3	11.5	87,300	I	2.013
G-LF-13	82.7	12.0	23,800	none	†
G-LF-12	89.6	13.0	14,700	none	†
G-LF-9	103.4	15.0	6,100	none	†
G-LF-39ac	45.4	6.6	636,700	none	†
G-LF-42ac	45.5	6.6	761,700	none	†
G-LF-43ac	49.4	7.2	2,292,100	none	†
G-LF-40ac	50.4	7.3	584,400	none	†
G-LF-34ac	51.7	7.5	510,500	none	†
G-LF-45ac	60.3	8.8	252,800	I	1.524
G-LF-36ac	65.7	9.5	>10,000,000	†	†
G-LF-31ac	68.3	9.9	692,100	none	†
G-LF-38ac	70.2	10.2	30,700	I	6.260
G-LF-35ac	73.3	10.6	204,300	none	†
G-LF-37ac	73.6	10.7	508,900	none	†
G-LF-26ac	79.6	11.5	52,900	none	†
G-LF-44ac	86.0	12.5	28,400	none	†

† Not Applicable
†† The flaw was of substantial size.

Flaw Type:
I Semi elliptical flaw originating at the surface
II Embedded internal circular flaw

R = 0.1
f = 10 Hz

TABLE 8

FATIGUE TEST RESULTS OF LOST-FOAM Al-Si 319 SAMPLES AT ROOM TEMPERATURE AND IN 99% CONTROLLED RELATIVE HUMIDITY

Specimen I.D.	Maximum Stress MPa	ksi	Cycles to Failure	Initial Flaw Depth, a_o (mm)
machined and polished specimens				
Al-T2-24	86.0	12.5	>10,000,000	†
Al-T3-319	90.0	13.0	2,184,719	0.75
Al-T3-317	90.0	13.0	1,343,085	0.83
Al-T2-26	93.0	13.5	>10,000,000	0.60
Al-T2-28	93.0	13.5	617,430	0.90
Al-T3-311	93.0	13.5	443,090	1.20
Al-T2-13	97.0	14.0	747,700	0.77
Al-T2-20	97.0	14.0	1,917,300	0.63
Al-T2-32	97.0	14.0	375,400	1.22
Al-T2-22	103.0	15.0	972,400	0.73
Al-T3-312	103.0	15.0	325,450	0.25
Al-T3-323	103.0	16.0	272,660	1.11
Al-T3-314	110.0	16.0	272,660	0.72
Al-T3-322	110.0	16.0	222,610	1.45
Al-T3-315	117.0	17.0	121,010	0.78
Al-T2-28ac	86.0	12.5	>10,000,000	0.90
Al-T2-21ac	90.0(32.4)††	13.0(4.7)††	6,279,900	0.20
Al-T2-20ac	93.0	13.5	268,600	0.63
Al-T2-22ac	93.0	13.5	>10,000,000	†
Al-T3-316ac	93.0	13.5	>10,000,000	†
Al-T3-318ac	97.0	14.0	2,514,540	0.45
Al-T3-317ac	97.0	14.0	5,671,410	0.83
Al-T2-26ac	103.0	15.0	560,270	0.60
Al-T3-312ac	103.0	15.0	2,748,310	0.25
Al-T3-315ac	110.0	16.0	592,410	0.78
Al-T3-319ac	110.0	16.0	408,950	*
Al-T3-313ac	117.0	17.0	769,240	0.35

† Not Applicable.
†† Grip end failure (true nominal stress in the grip net section).
* The required information was unavailable.

R = 0.1
f = 10 Hz

TABLE 9

FATIGUE TEST RESULTS OF LOST-FOAM Al-Si 319

SAMPLES AT 300 °F TEMPERATURE

Specimen I.D.	Maximum Stress MPa	ksi	Cycles to Failure	Initial Flaw Depth, a_o (mm)
machined and polished specimens				
Al-T1-10	80.0(28.8)††	11.5(4.1)††	9,944,800	0.86
Al-T1-15	86.0	12.0	>10,000,000	†
Al-T1-17	86.0	12.5	>10,000,000	†
Al-T2-17	86.0	12.5	>10,000,000	†
Al-T2-23	90.0	13.0	3,097,000	0.33
Al-T2-101	90.0	13.0	>10,000,000	†
Al-T1-18	90.0(32.4)††	13.0(4.7)††	6,315,500	1.11
Al-T1-14	90.0	13.0	807,300	0.82
Al-T3-321	97.0	14.0	853,650	*
Al-T3-320	103.0	15.0	442,550	*
Al-T3-318	110.0	16.0	286,940	0.45
Al-T1-10ac	76.0	11.0	>10,000,000	†
Al-T1-17ac	80.0	11.5	>10,000,000	†
Al-T1-14ac	80.0	11.5	986,100	*
Al-T1-13ac	83.0	12.0	967,700	†
Al-T1-2ac	83.0	12.0	1,413,300	0.32
Al-M-1ac	83.0	12.0	1,113,900	*
Al-M-11ac	83.0	12.0	1,864,100	*
Al-T2-23ac	90.0	13.0	2,201,600	0.33
Al-T2-101ac	90.0	13.0	1,084,000	0.5
Al-T3-325ac	97.0(34.9)††	14.0(5.0)††	4,919,100	*
Al-T3-323ac	103.0(37.0)††	15.0(5.4)††	1,779,800	*

† Not Applicable.
†† Grip end failure (true nominal stress in the grip net section).
* The required information was unavailable.

R = 0.1
f = 10 Hz

TABLE 10

INITIAL STRESS INTENSITY FACTORS AND PREDICTED LIVES OF EMPTY-CAVITY NODULAR CAST IRON.

Specimen I.D.	Smax (MPa)	a_o (mm)	$^1\Delta K_o$ (MPa $\sqrt{m}$)	N_f (cycles) (actual)	N_p (cycles) (predicted)
N-EC-7	379.2	0.165*	4.94	6,213,400	†
N-EC-9	355.1	0.417*	7.36	2,039,400	†
N-EC-29	382.7	0.074	12.71	1,105,500	759,730
N-EC-20	372.3	0.140	14.49	675,700	419,570
N-EC-4	344.0	0.200	15.50	339,500	219,200
N-EC-8	413.7	0.120	15.55	219,200	200,260
N-EC-3	362.0	0.241	16.26	339,500	250,910
N-EC-36	368.9	0.240	16.52	185,700	179,065
N-EC-18	349.5	0.320	16.87	977,300	226,890
N-EC-26	368.9	0.267	16.95	302,300	183,605
N-EC-24	375.8	0.260	17.15	210,000	161,690
N-EC-31	375.8	0.300	17.81	251,900	130,560
N-EC-38	368.9	0.530	20.31	159,000	60,555
N-EC-1	393.0	0.420	20.39	48,200	51,290
N-EC-25	358.5	0.610	20.55	144,300	60,280
N-EC-23	348.2	0.929	22.63	44,300	31,695
N-EC-11	349.6	1.333	26.01	31,500	10,995
N-EC-13	355.1	5.700	**	17,000	†

R = 0.1
f = 10 Hz

1 Based on the average aspect ratio of 0.913 of the initial flaw.

* Based on an embedded circular flaw as found in Appendix A.

** The flaw occupied more than 50% of the cross-section which invalidated the semi-elliptical flaw stress intensity model .

† A life prediction for this type of flaw was not performed due to lack of information regarding the behavior of the crack growth.

TABLE 11

INITIAL STRESS INTENSITY FACTORS AND PREDICTED LIVES OF LOST-FOAM NODULAR CAST IRON.

Specimen I.D.	Smax (MPa)	a_o (mm)	ΔK_o** (MPa $\sqrt{m}$)	N_f (cycles) (actual)	N_p (cycles) (predicted)
N-LF-14ac	340.5	0.367	6.62	1,312,100	†
N-LF-12ac	373.3	0.435	7.90	469,400	†
N-LF-38	310.3	0.960	9.76*	3,361,200	†
N-LF-22ac	330.5	0.889	10.01	2,613,400	†
N-LF-39	331.0	0.257	15.11	335,600	282,760
N-LF-9ac	197.7	1.180	15.69	615,700	543,830
N-LF-21	379.2	0.210	16.44	305,900	185,525
N-LF-10	379.2	0.250	17.17	681,900	270,950
N-LF-11	365.4	0.311	17.51	366,700	210,129
N-LF-6	344.8	0.470	18.42	328,300	169,070
N-LF-18	379.2	0.429	19.77	295,100	125,670
N-LF-20	448.2	0.225	19.77	134,500	94,760
N-LF-2	413.7	0.333	20.18	101,600	104,815
N-LF-19	517.1	0.170	21.25	52,300	61,720
N-LF-23	344.8	1.044	23.39	666,700	77,360
N-LF-4ac	263.8	1.922	23.87	2,097,700	101,293
N-LF-30	372.3	0.899	24.01	59,700	69,690
N-LF-15ac	328.1	1.376	25.59	397,700	69,280
N-LF-8	482.7	0.510	26.37	46,000	43,895
N-LF-3	482.7	0.513	26.41	25,400	43,950
N-LF-13	413.7	0.846	26.59	85,400	77,560
N-LF-26	310.3	2.267	31.37	37,400	19,424
N-LF-17ac	578.4	0.432	32.38	5,100	22,150
N-LF-29	389.6	1.834	33.93	22,500	15,760

R = 0.1
f = 10 Hz

** Based on the average aspect ratio of 0.913 of the initial flaw.

* Based on an embedded circular flaw as found in Appendix A.

† A life prediction for this type of flaw was not performed due to lack of information regarding the behavior of the crack growth.

TABLE 12

INITIAL STRESS INTENSITY FACTORS AND PREDICTED LIVES OF GRAY CAST IRON.

Specimen I.D.	Smax (MPa)	a_o (mm)	ΔK_o ** (MPa $\sqrt{m}$)	N_f (cycles) (actual)
G-EC-25	69.0	3.120	10.29	22,700
G-EC-30	96.5	2.263	9.73	170,500
G-EC-10	103.4	1.990	9.48	24,600
G-LF-16	77.6	2.013	7.17	87,300
G-EC-18	100.0	0.749	6.10	47,900
G-LF-45ac	60.3	1.524	4.93	252,800
G-LF-2	75.8	5.080	†	1,500
G-LF-38ac	70.2	6.260	†	30,700

R = 0.1
f = 10 Hz

** Based on an assumed aspect ratio of 0.913 of the initial flaw.

† The initial flaw depth was not within the constraints of the stress intensity model (see Appendix A).

TABLE 13
INITIAL STRESS INTENSITY FACTORS AND
PREDICTED LIVES OF Al-Si 319 ALLOY

Specimen I.D.	Smax (MPa)	a_o (mm)	ΔK_o** (MPa $\sqrt{m}$)	N_f (cycles) (actual)	N_p (cycles) (predicted)
Room Temperature					
T2-21ac	90.0	0.20	1.598	6,279,900	3,522,000
T3-312ac	103.0	0.25	5.205	2,748,310	2,015,000
T2-13	97.0	0.77	5.639	747,700	954,000
T3-318ac	97.0	0.45	5.691	2,514,540	1,549,000
T2-28	93.0	0.90	5.714	617,430	918,000
T2-22	103.0	0.73	5.882	972,400	840,000
T2-20ac	93.0	2.10	5.954	268,600	217,000
T3-314	110.0	0.72	6.254	272,660	699,000
T3-313ac	117.0	0.35	6.438	769,240	1,076,000
T3-311	93.0	1.20	6.448	443,090	646,000
T2-26ac	103.0	0.60	6.510	560,270	1,011,000
T3-317ac	97.0	0.83	6.686	5,671,410	882,000
T3-315	117.0	0.95	6.832	121,010	434,000
T3-323	103.0	1.11	6.890	222,081	527,000
T3-315ac	110.0	0.78	7.445	592,410	645,000
T3-322	110.0	1.45	8.442	222,610	294,000
300°F					
T1-10	28.8	0.86	1.909	9,944,800	32,465,000
T1-18	32.4	1.11	2.319	6,315,500	16,922,000
T1-2ac	83.0	0.32	4.464	1,413,300	3,223,000
T2-23	90.0	0.33	4.619	3,097,000	2,471,000
T2-23	90.0	0.33	4.879	2,201,600	2,781,105
T2-101ac	90.0	0.50	5.425	1,084,000	1,177,000
T1-14	90.0	0.82	5.885	807,300	1,119,000
T3-318	110.0	0.45	6.115	286,940	312,215

R = 0.1
f = 10 Hz

** Based on the average aspect ratio of 0.950 of the initial flaw.

* Based on an embedded circular flaw as found in Appendix A.

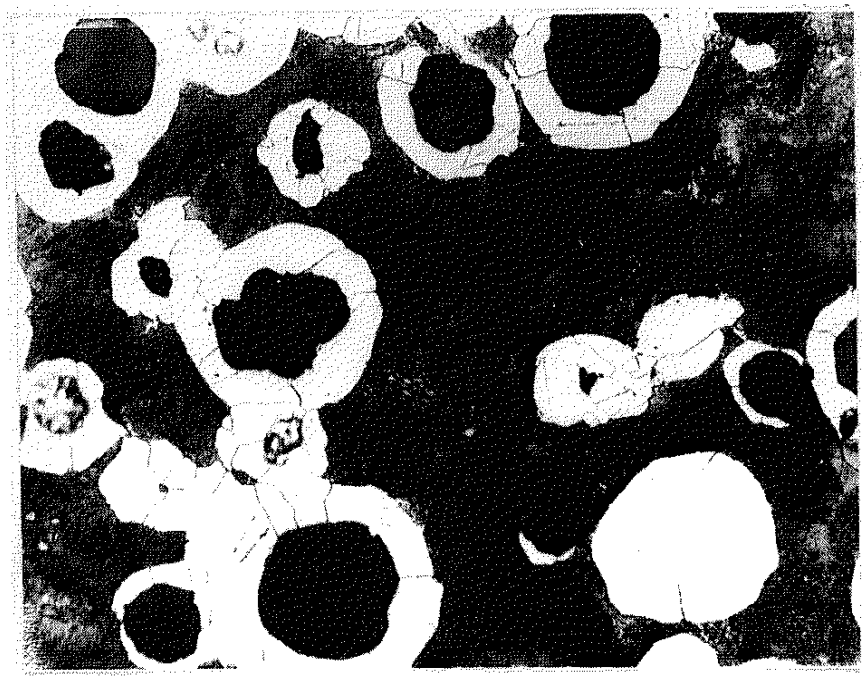

Fig. 1 Microstructure of empty-cavity nodular cast iron. 400x. Etchant : 2% nital

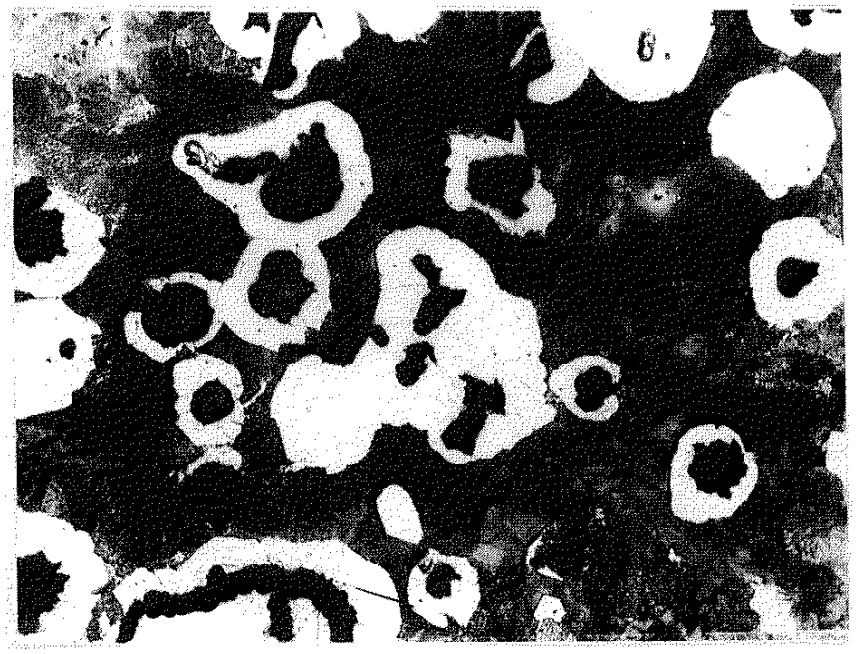

Fig. 2 Microstructure of lost-foam nodular cast iron. 400x. Etchant : 2% nital

Fig. 3 Microstructure of empty-cavity gray cast iron. 400x. Etchant : 2% nital

Fig. 4 Microstructure of lost-foam gray cast iron. 400x. Etchant : 2% nital

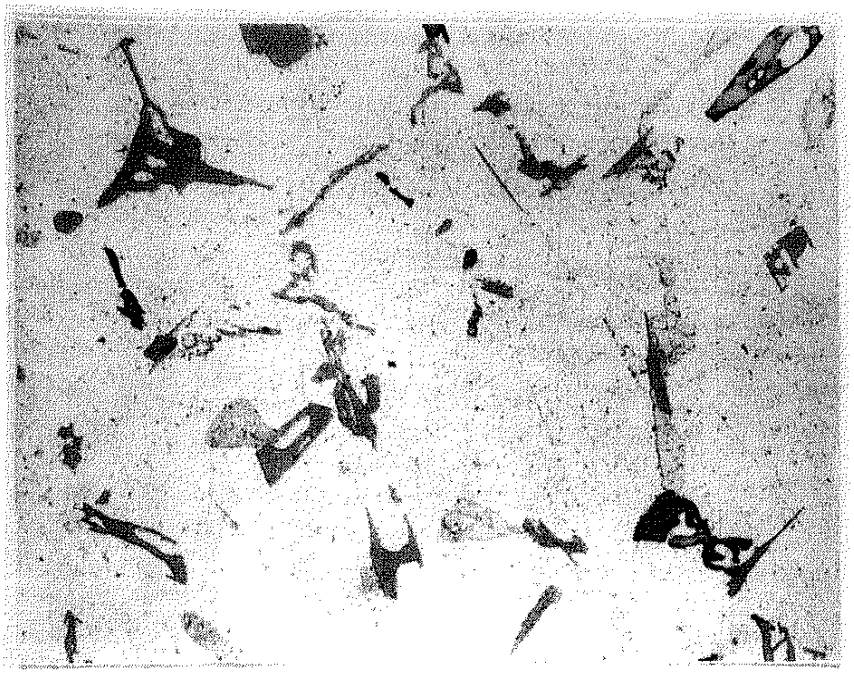

Fig. 5 Microstructure of aluminum-silicon 319 alloy. 400x. Etchant : Keller's Etch

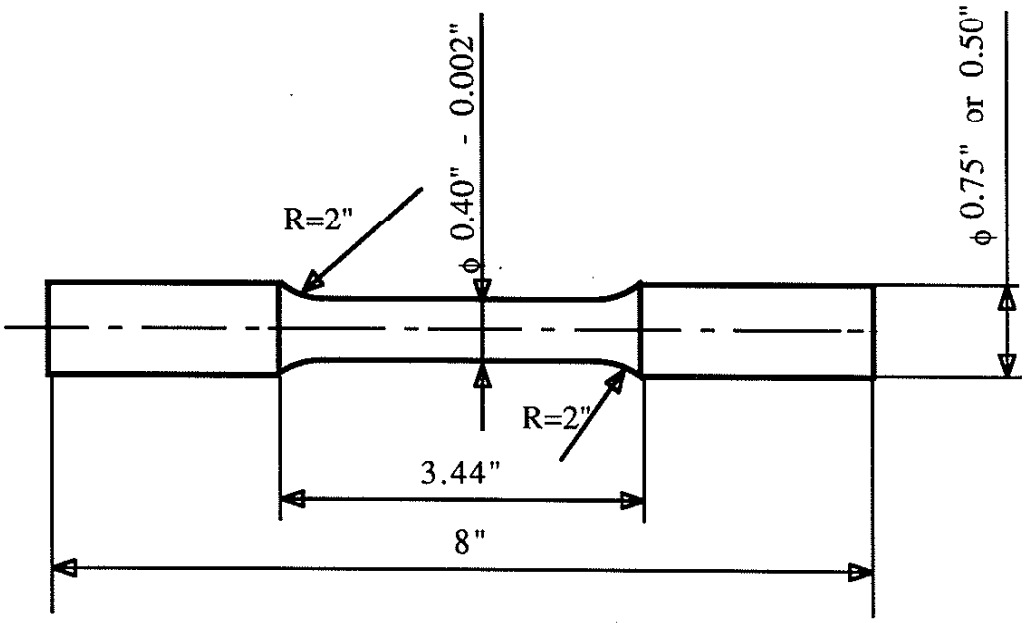

Fig. 6 Dimensions of the cast iron specimen in the machined condition.

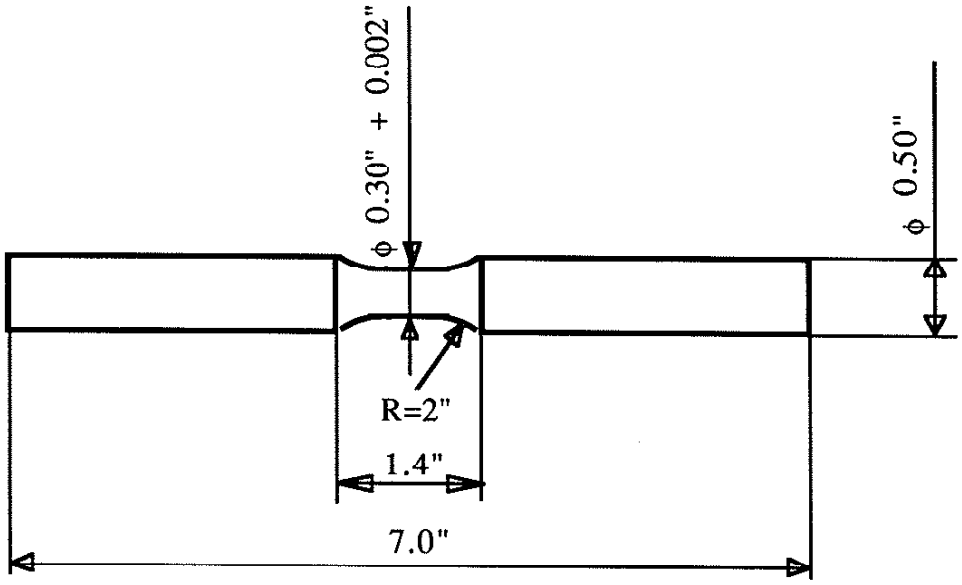

Fig. 7 Dimensions of the aluminum-silicon test specimen for room temperature and elevated temperature fatigue tests.

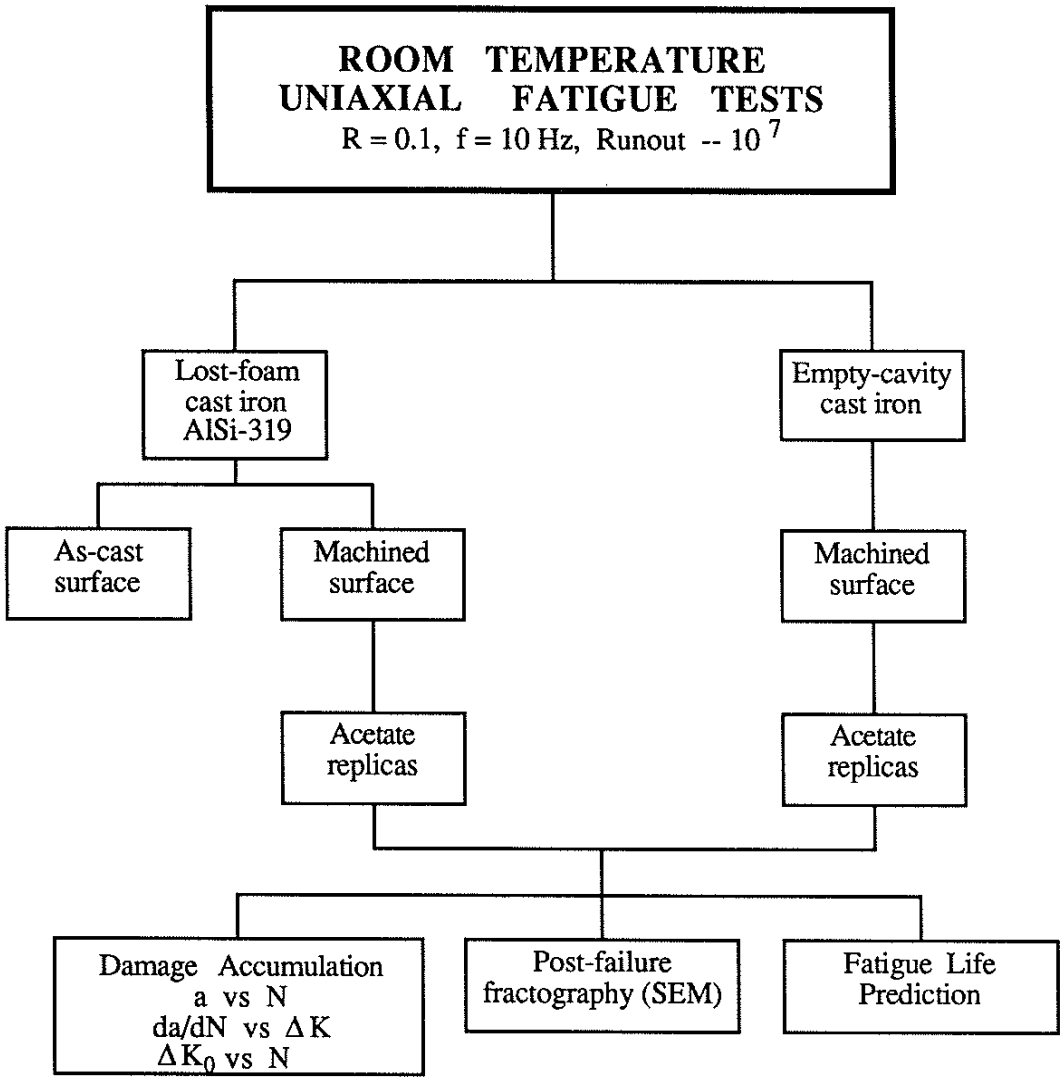

Fig. 8 Block diagram of fatigue testing.

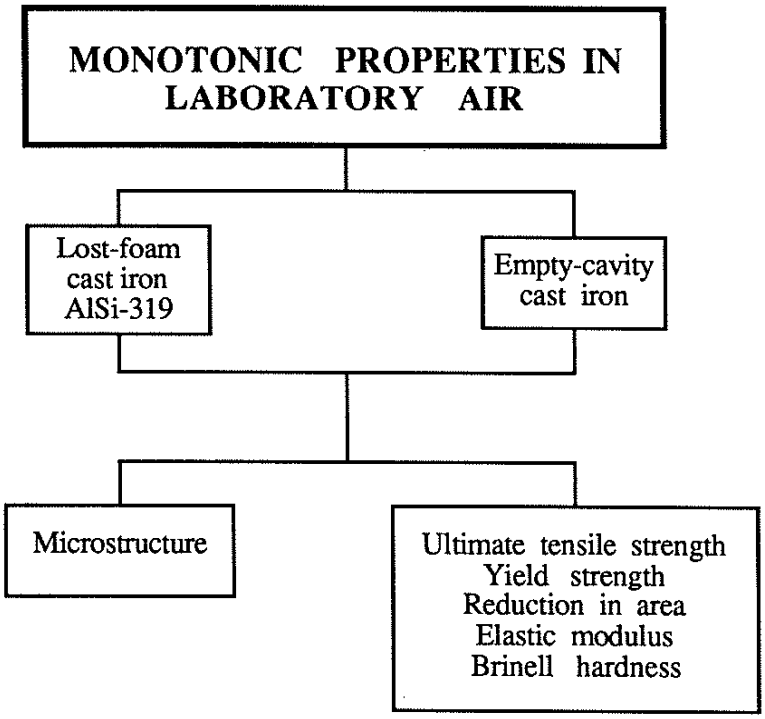

Fig. 9 Block diagram for monotonic testing.

Fig. 10 SEM fractograph of a typical semi-elliptical surface flaw in cast iron (Type I). 100x. The scale indicates a division of 100 μm.

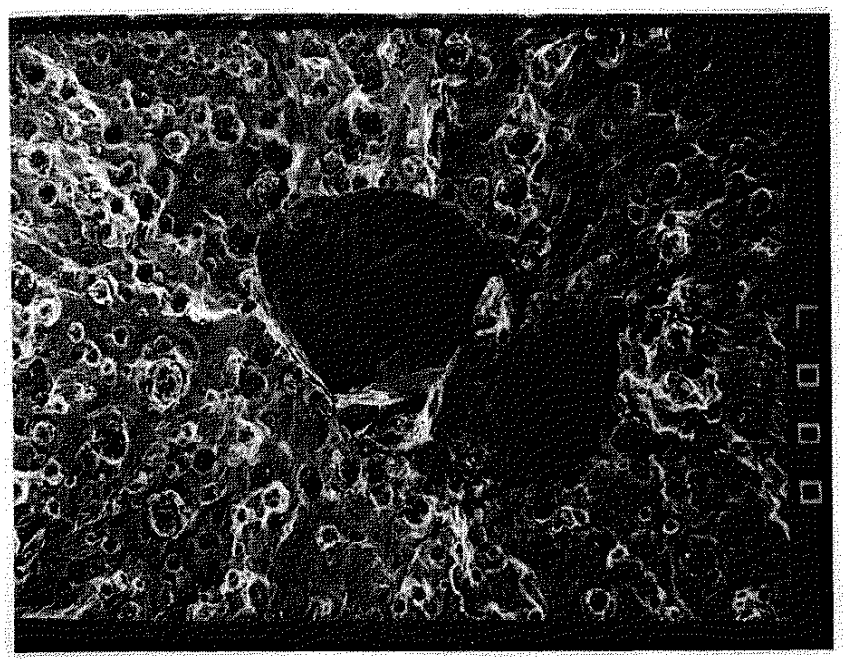

Fig. 11 SEM fractograph of a typical spherical-internal flaw in cast iron (Type II). 100x.

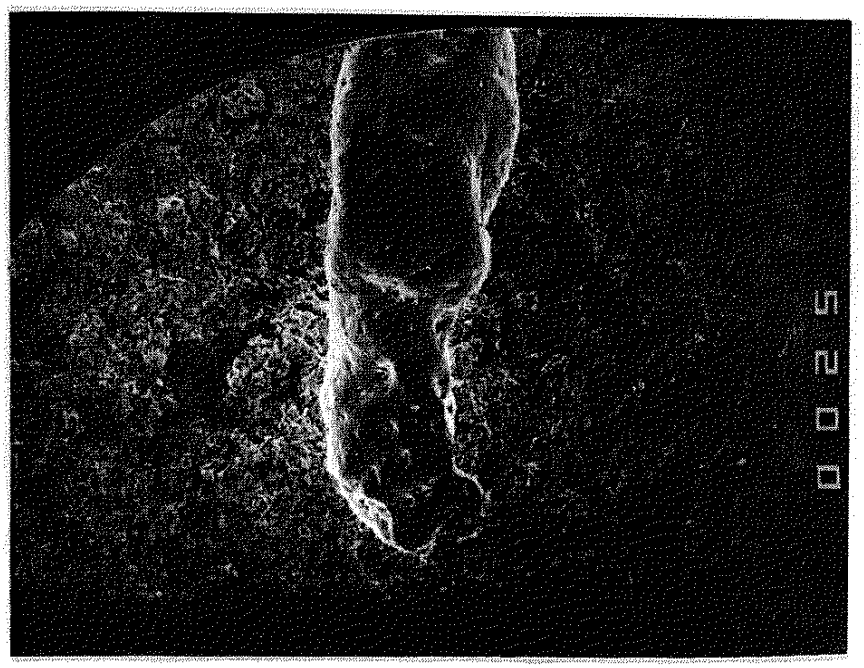

Fig. 12 SEM fractograph of a typical cylindrical surface flaw in cast iron (Type III). 20x.

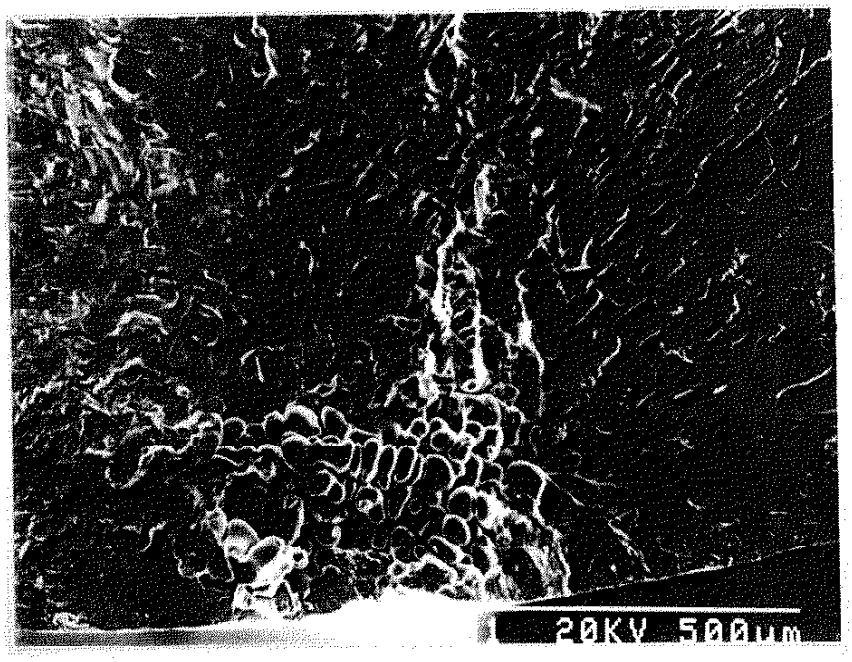

Fig. 13 SEM fractograph of a typical semi-elliptical surface flaw in aluminum-silicon alloy (Type I). 100x.

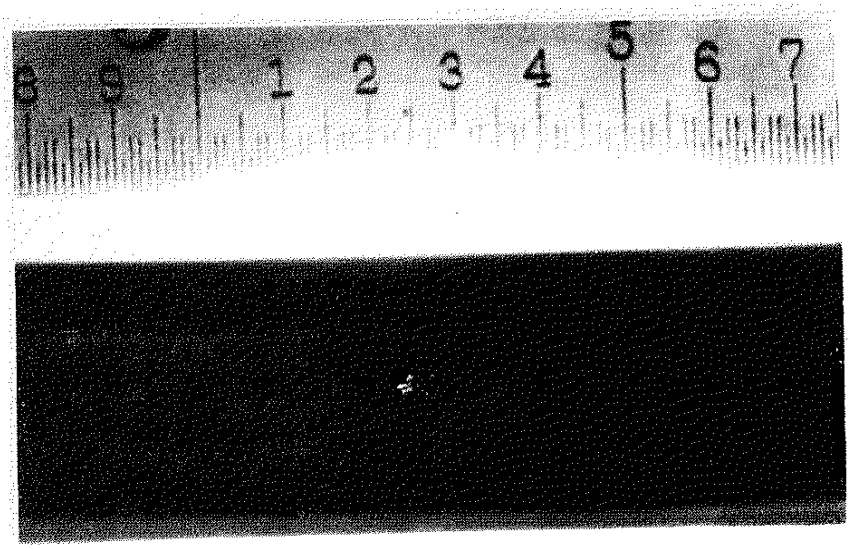

Fig. 14 Macrograph of a flaw on the surface of specimen G-LF-15 before testing. The numbers indicate a division of 0.1 inch. 4.5X.

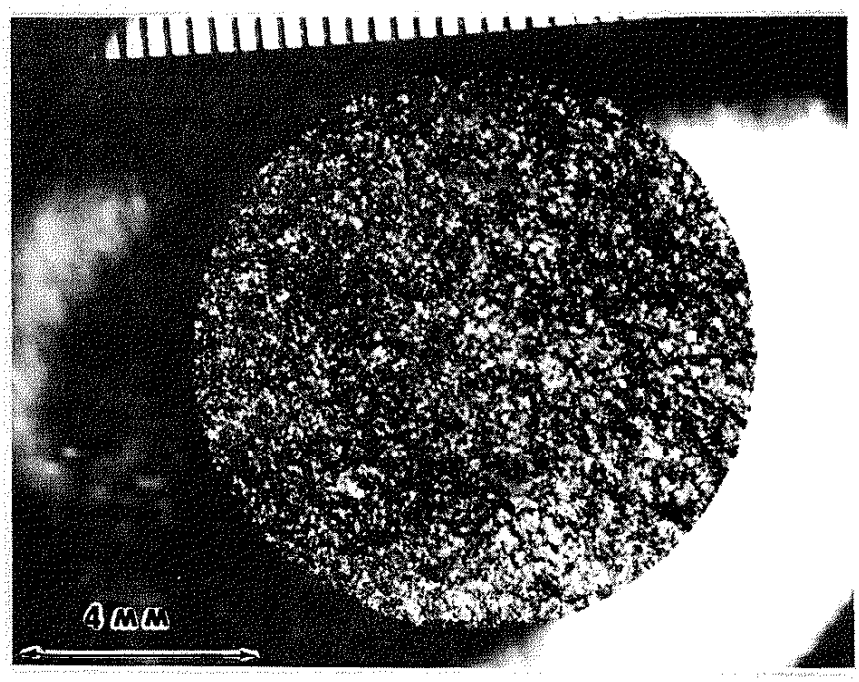

Fig. 15 Macrograph of the fracture surface of specimen G-LF-15 after fatigue testing.

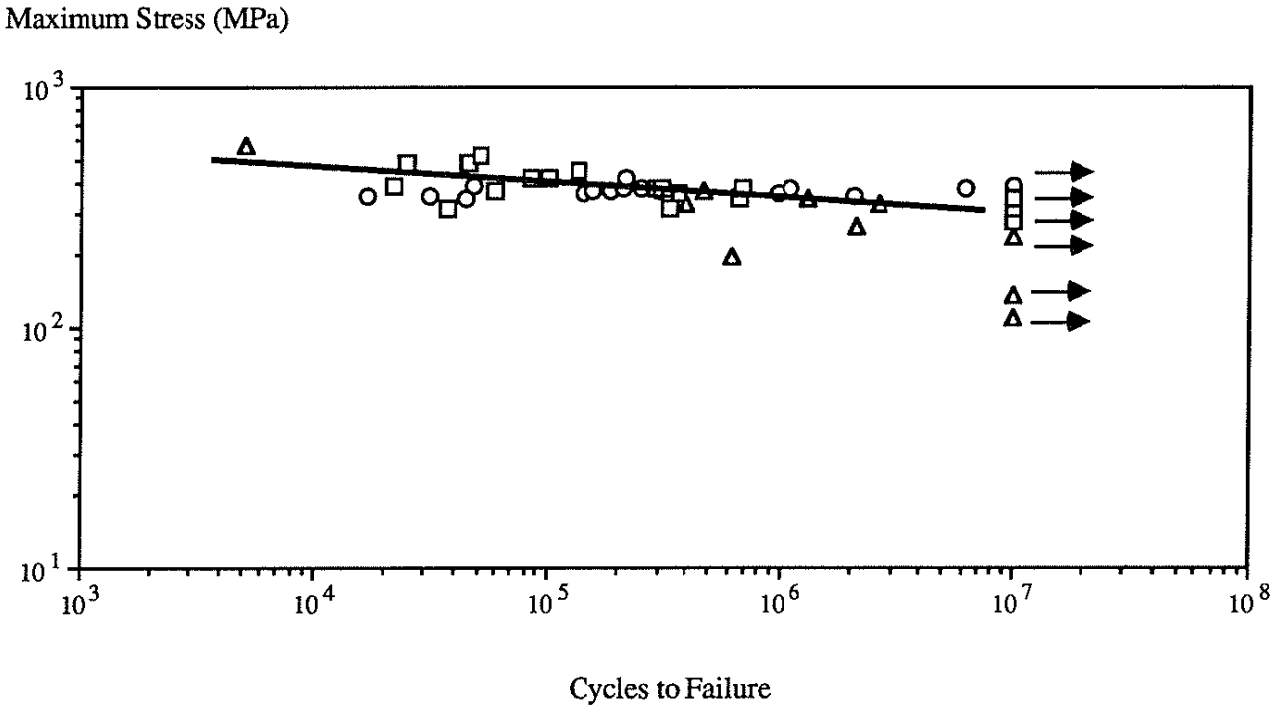

Fig. 16 Maximum stress versus cycles to failure curve for all nodular cast iron specimens. The arrows indicate runout.

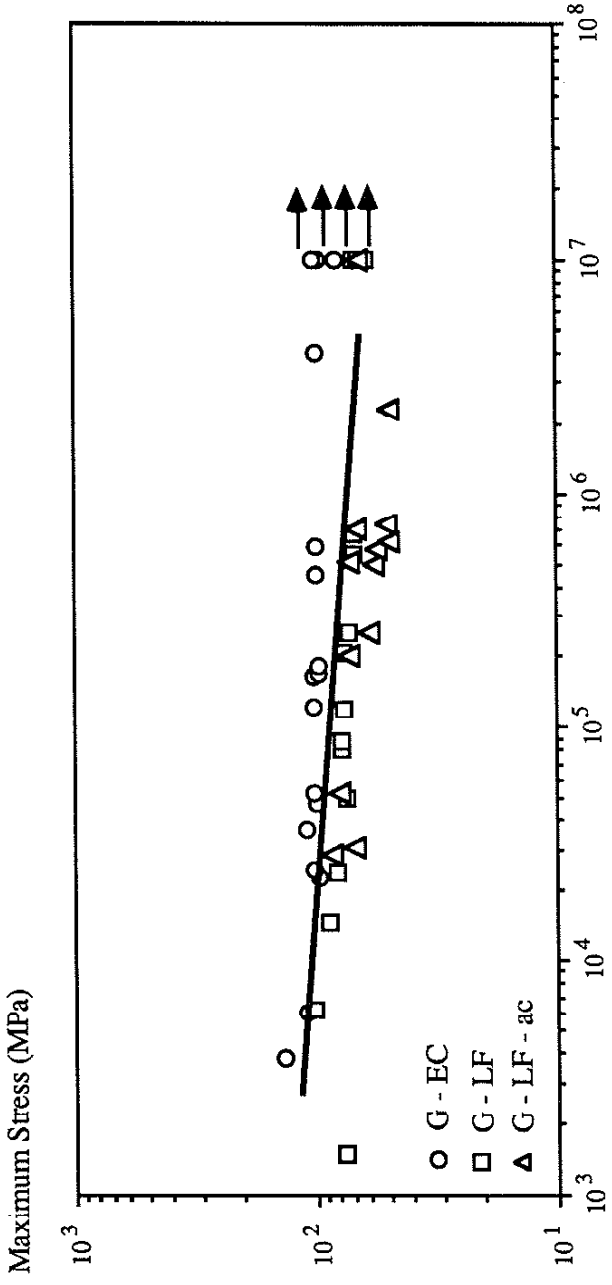

Fig. 17 Maximum stress versus cycles to failure curve for all gray cast iron specimens. The arrows indicate runout.

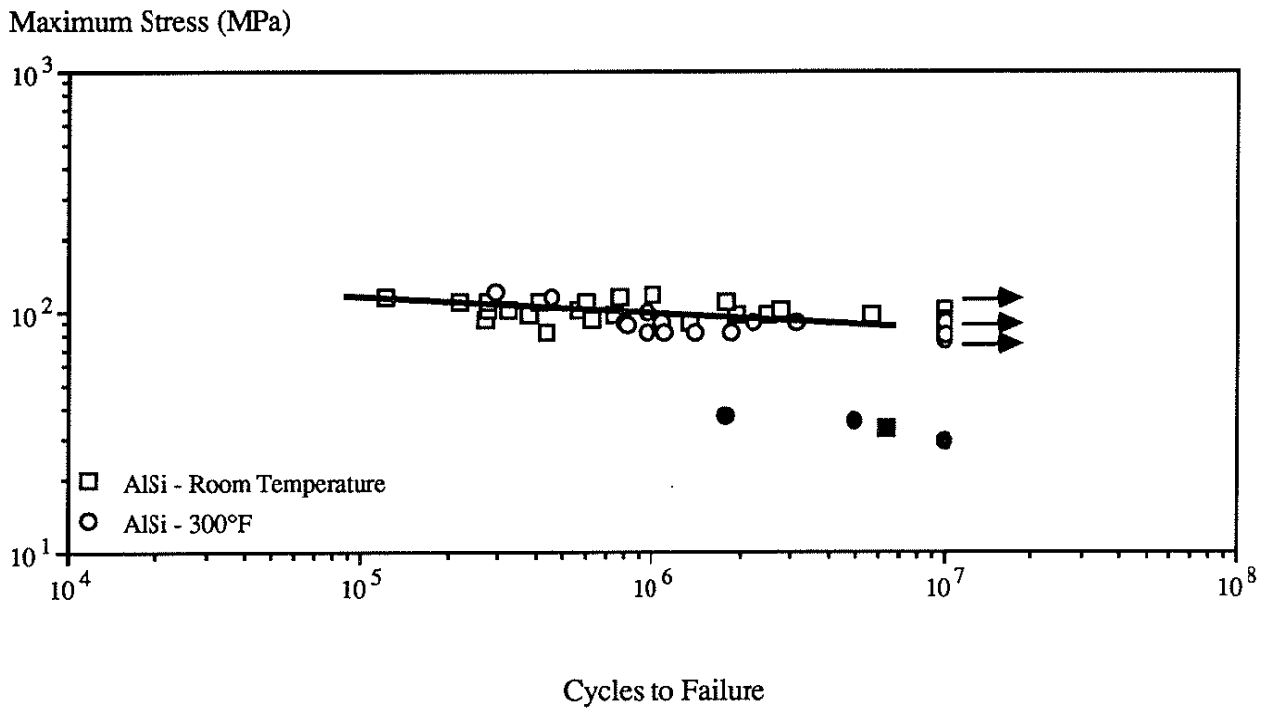

Fig. 18 Maximum stress versus cycles to failure curve for Aluminum-Silicon 319. The solid symbols represent grip-end failures and the arrows indicate runout.

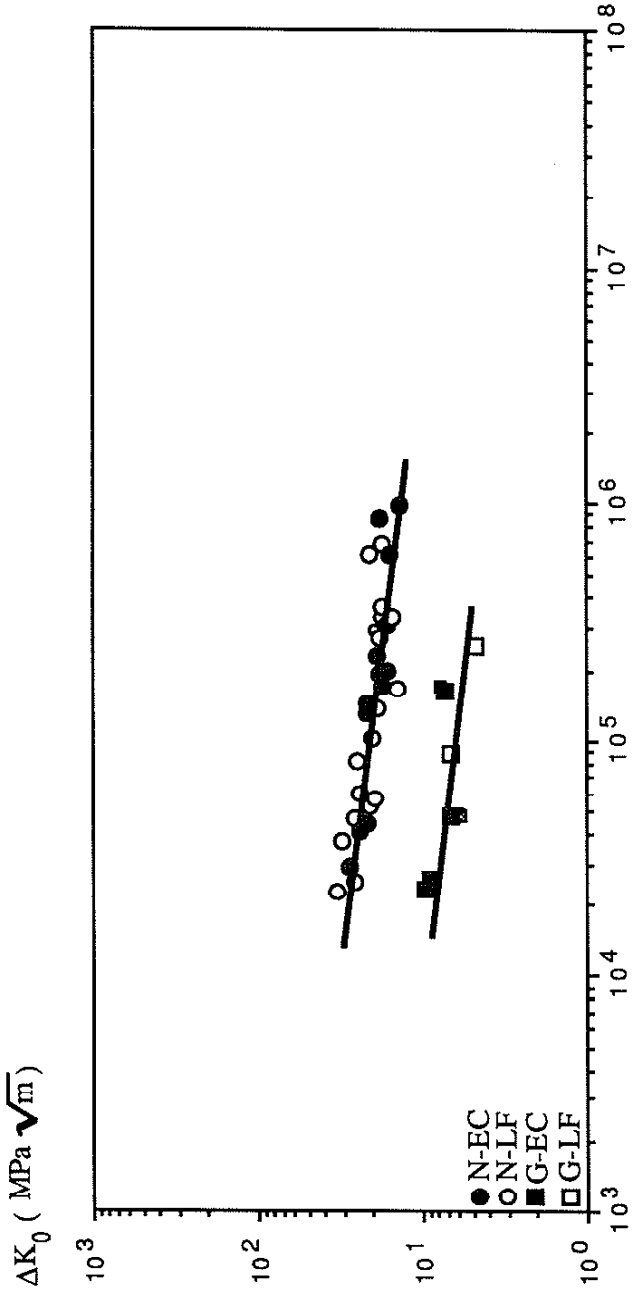

Fig. 19 Stress intensity factor versus cycles to failure curve for nodular and gray cast iron.

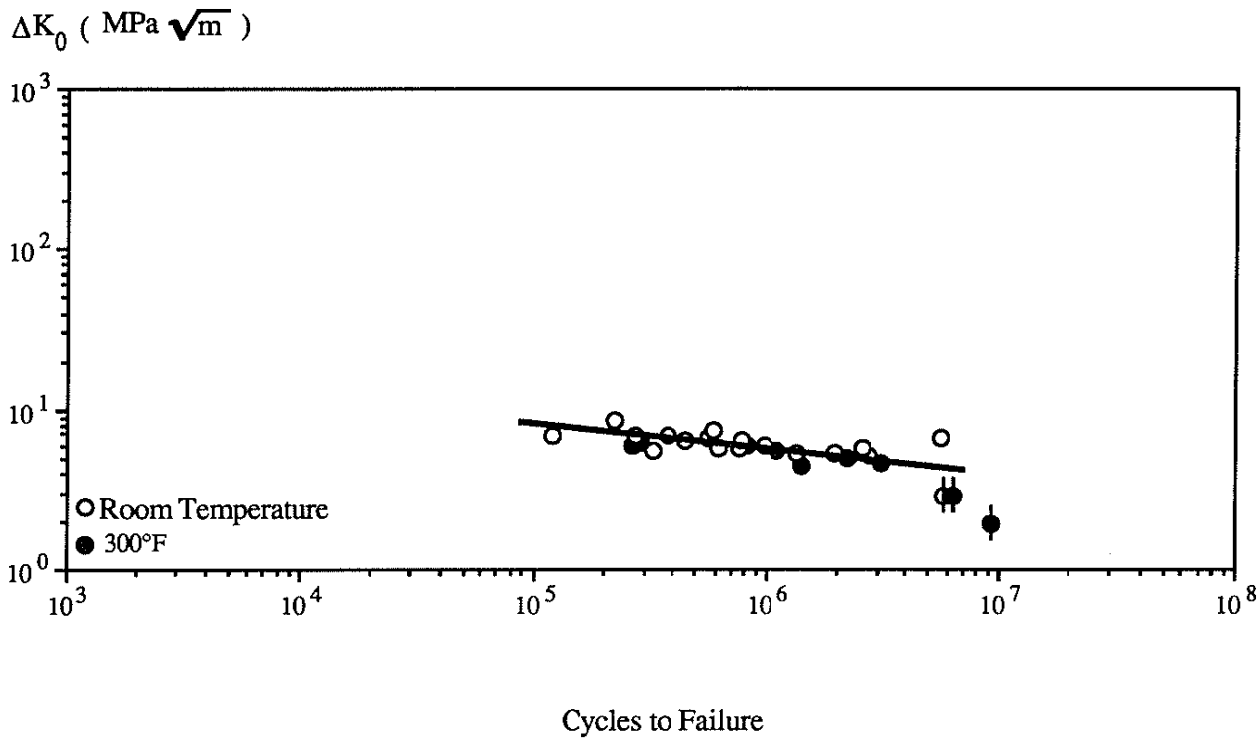

Fig. 20 Stress intensity factor versus cycles to failure curve for Aluminum-Silicon. A symbol with the vertical line indicates a grip-end failure.

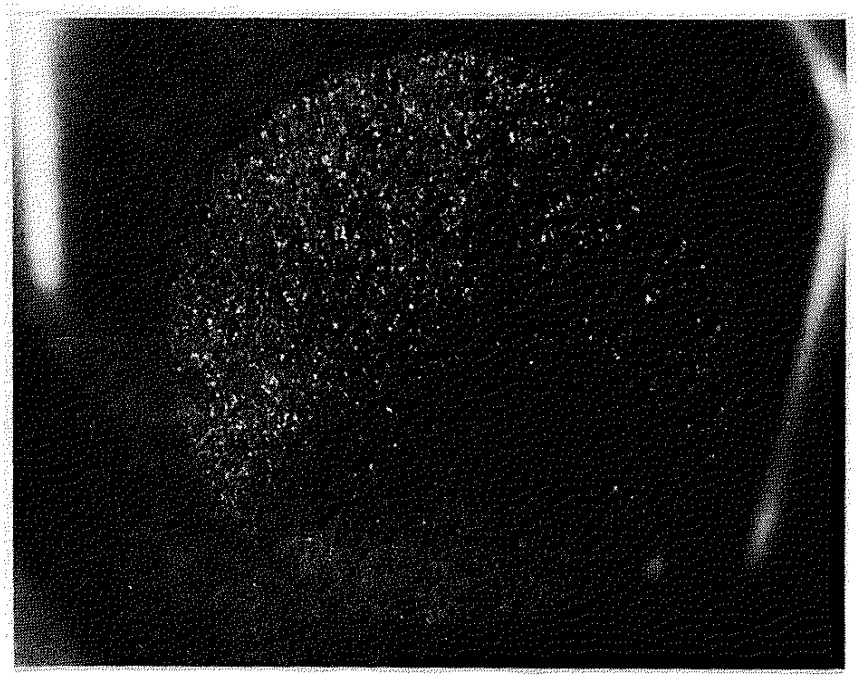

Fig. 21 Macrograph of a nodular cast iron (N-LF-10) fracture surface that initiated at a type I flaw. 7X.

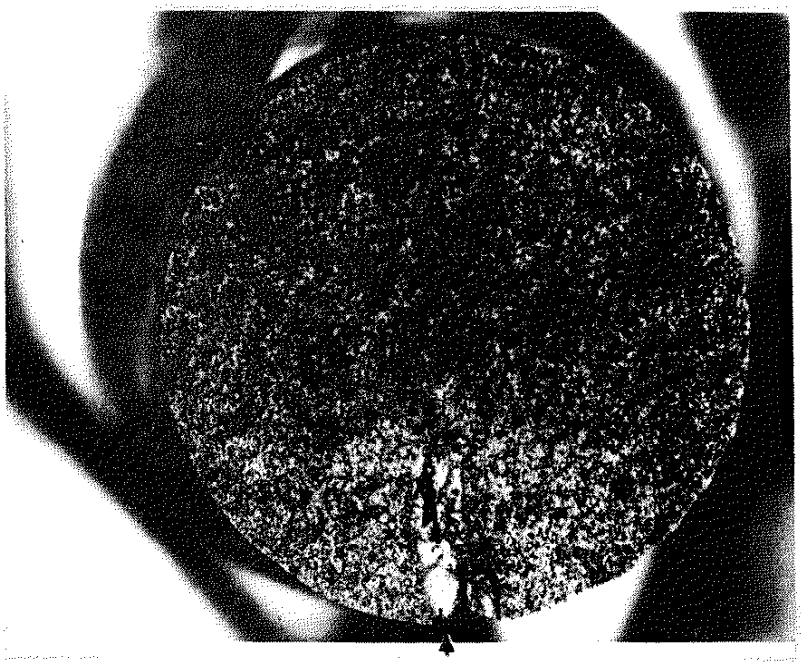

Fig. 22 Macrograph of a gray cast iron (G-EC-25) fracture surface that initiated at a type II flaw. 8X.

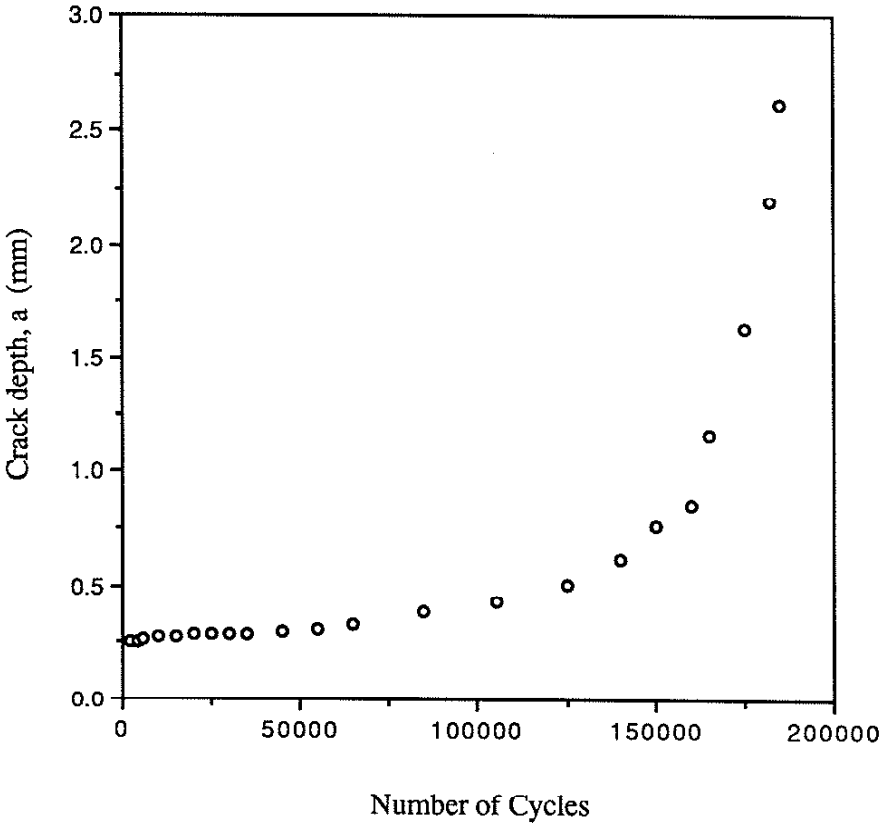

Fig. 23 Crack depth versus number of cycles from the replication of empty-cavity nodular cast iron (N-EC-36). Smax = 368.9 MPa; N_f = 185,700 cycles.

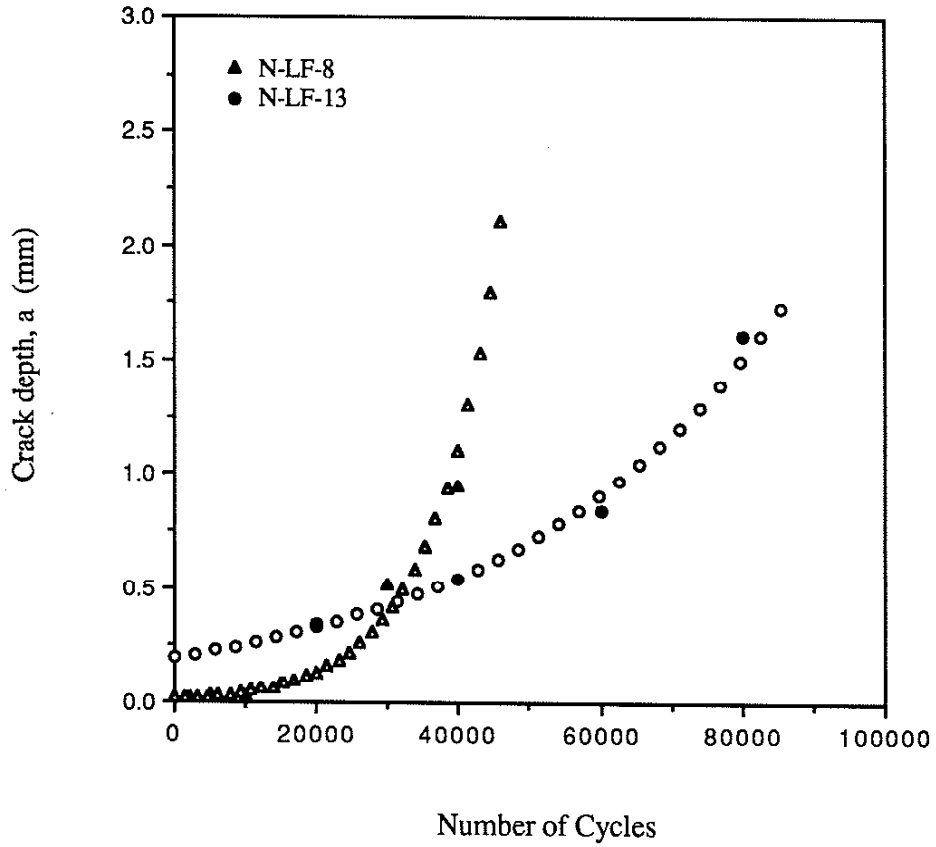

Fig. 24 Crack depth versus number of cycles from the replication of specimens N-LF-8 (Smax = 482.7 MPa; N_f = 46,000 cycles) and N-LF-13 (Smax = 413.7 MPa; N_f = 85,400 cycles). The white symbols indicate the exponential curve used to calculate da/dN.

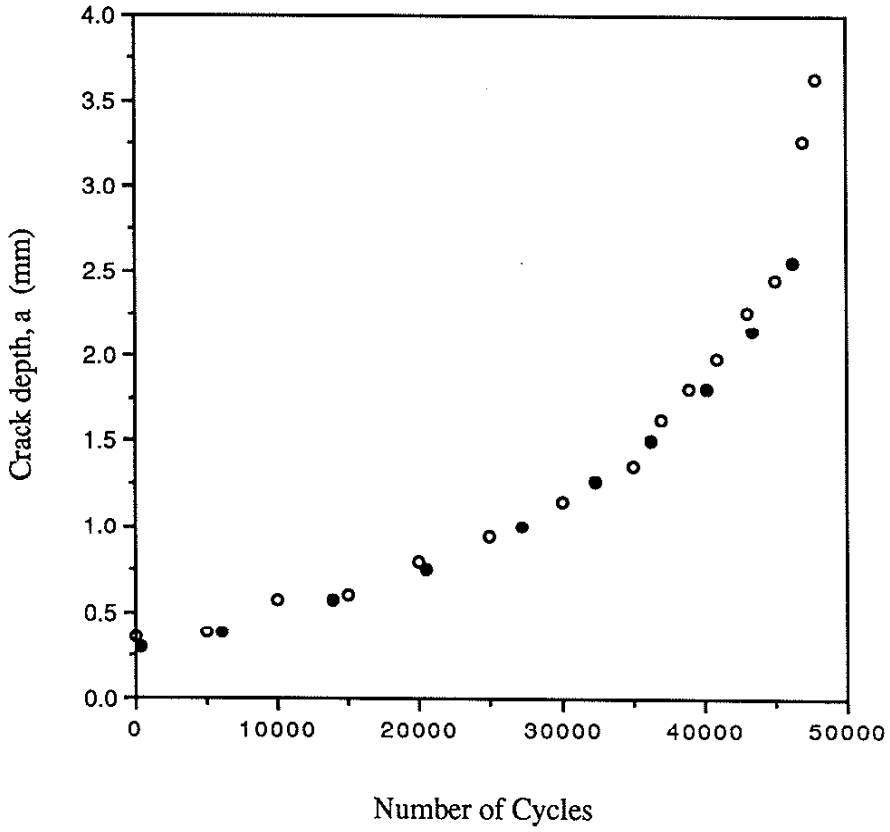

Fig. 25 Crack depth versus number of cycles from the replication of specimen G-EC-18. S_{max} = 100.0 MPa ; N_f = 47,900 cycles. The solid symbols indicate the exponential curve used to calculate da/dN.

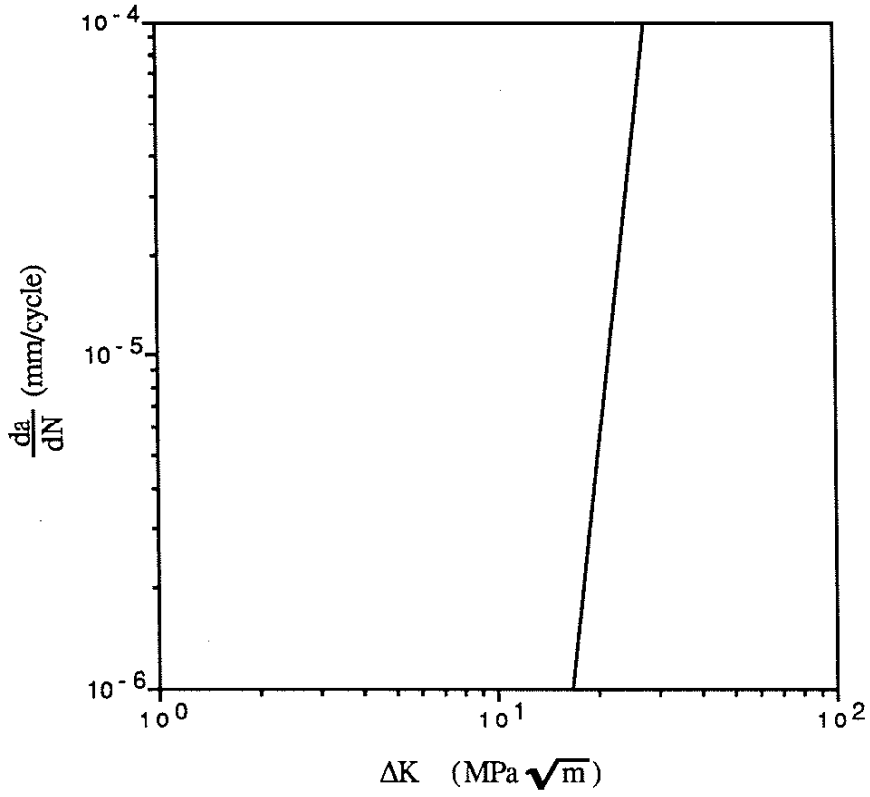

$da/dN = 1.0245 \times 10^{-20} (\Delta K)^{8.9775}$ (meters/cycle) R = 0.992

$C = 1.0245 \times 10^{-20}$ (meters / cycle)

m = 8.9775

Fig. 26 Crack growth rate versus change in stress intensity factor of empty-cavity nodular cast iron (N-EC-36).

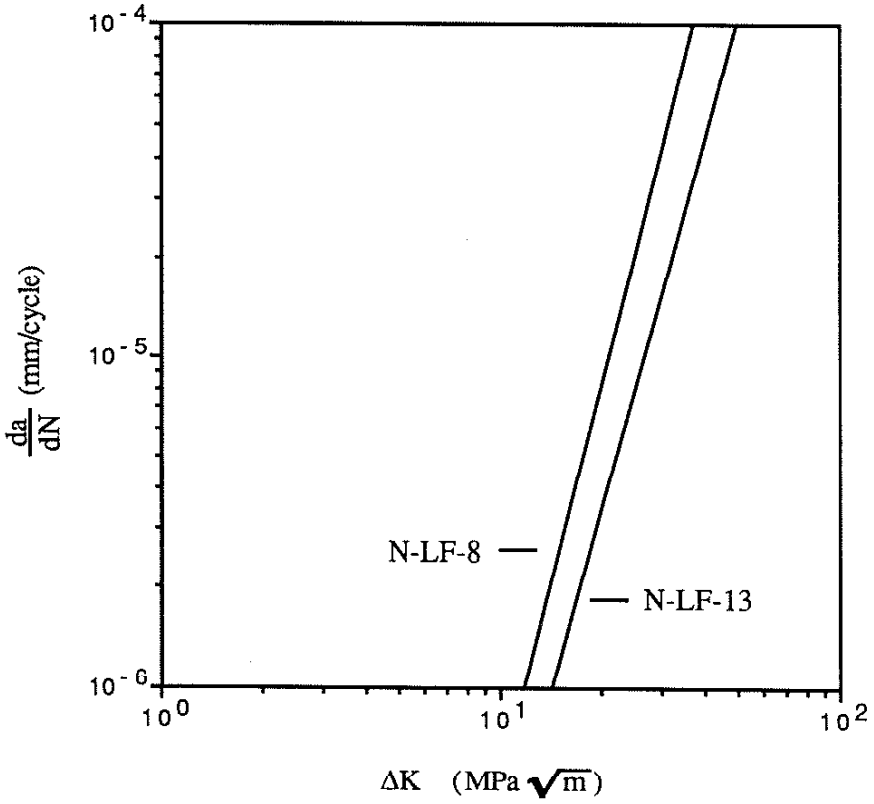

N-LF-8 : $da/dN = 5.2524 \times 10^{-14}(\Delta K)^{3.9859}$ (meters/cycle) R = 0.990

$C = 5.2524 \times 10^{-14}$ (meters / cycle)

m = 3.9859

N-LF-13 : $da/dN = 5.8522 \times 10^{-14}(\Delta K)^{3.6742}$ (meters/cycle) R = 0.993

$C = 5.8522 \times 10^{-14}$ (meters / cycle)

m = 3.6742

Fig. 27 Crack growth rate versus change in stress intensity factor of specimens N-LF-8 and N-LF-13.

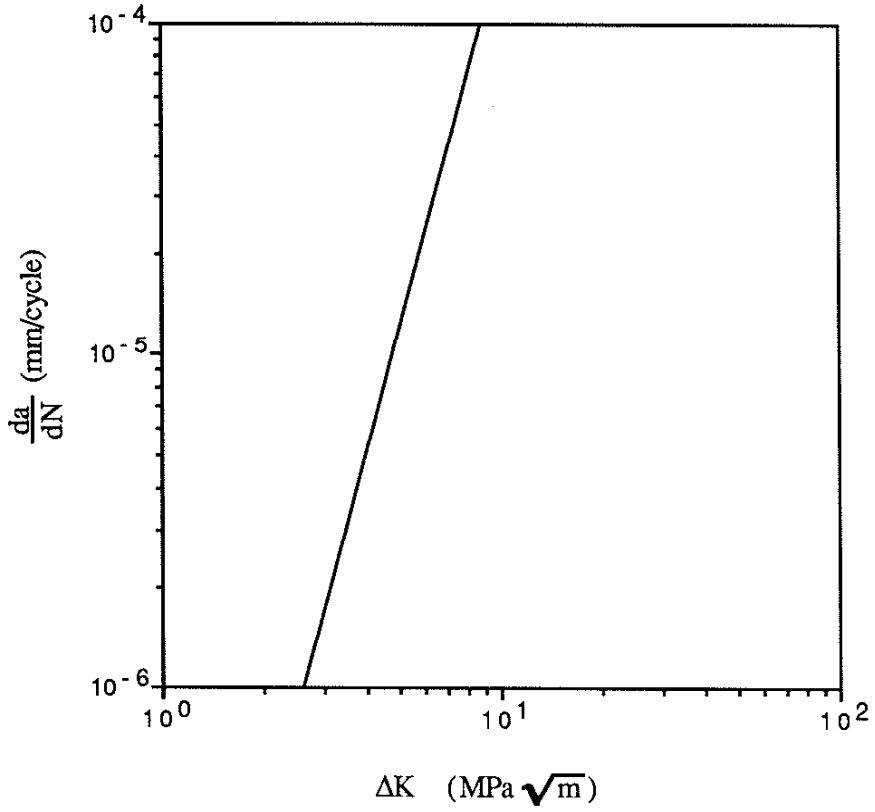

$da/dN = 2.9848 \times 10^{-11} (\Delta K)^{3.7110}$ (meters/cycle) R = 0.994

$C = 2.9848 \times 10^{-11}$ (meters / cycle)

m = 3.7110

Fig. 28 Crack growth rate versus change in stress intensity factor of specimen G-EC-18.

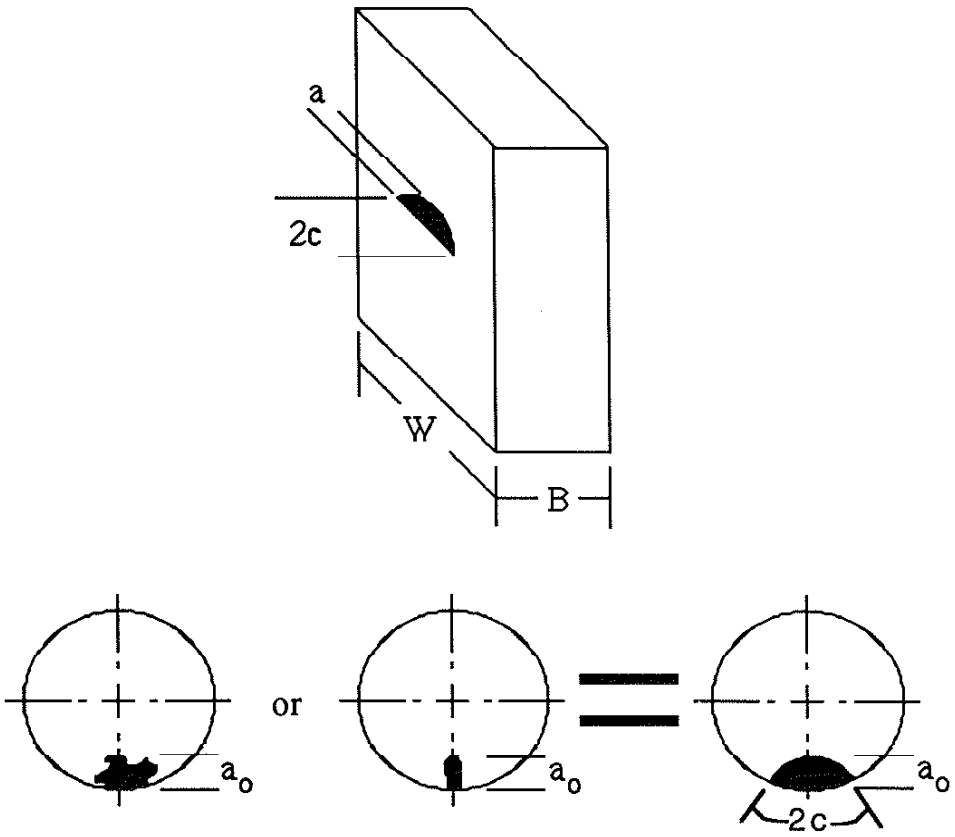

Fig. 29 Fracture mechanics model of a semi-elliptical surface flaw in tension. An equivalent rectangular specimen shape was assumed.

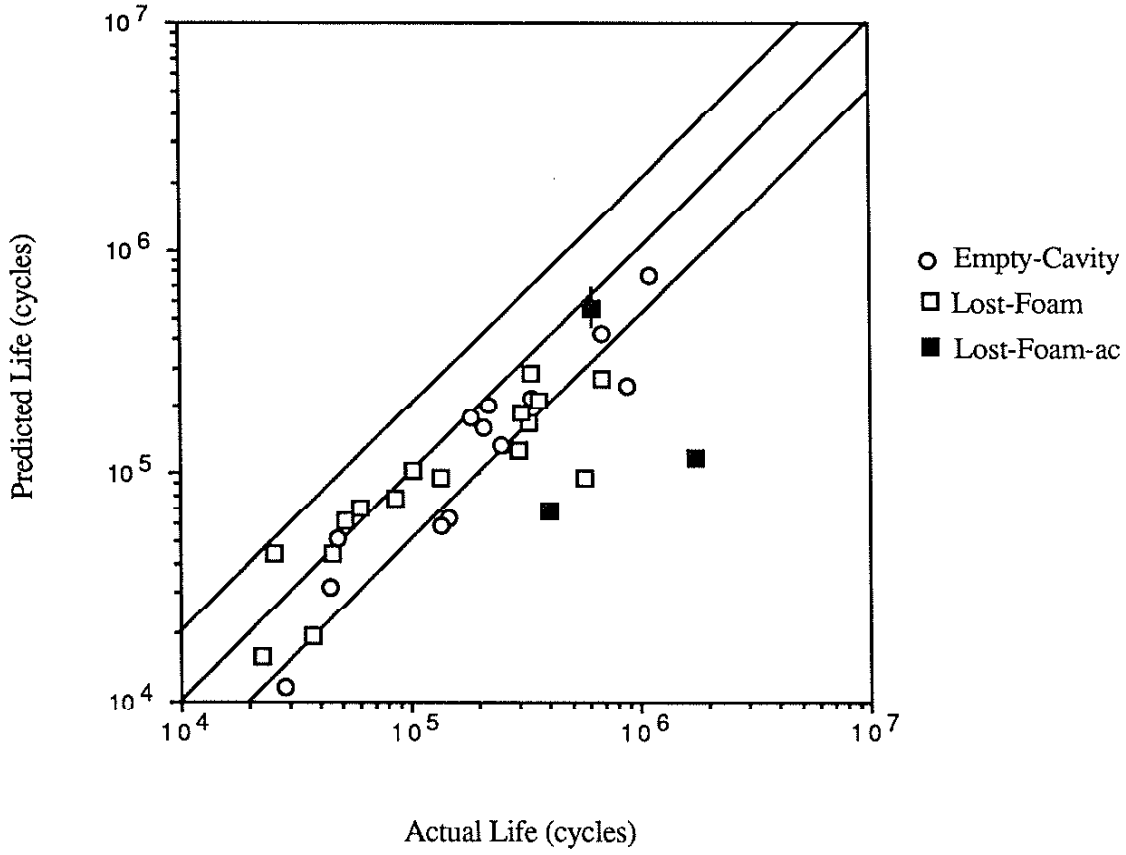

Fig. 30 Comparison of the predicted life and the actual life for empty-cavity and Lost-Foam Nodular cast iron. The lines to the left and right of the predicted = actual line (middle) indicates a factor of two. The symbol with the vertical line indicates a grip-end failure. Due to the dependance of the fatigue of gray cast iron on the carbon flakes, life predications were not performed.

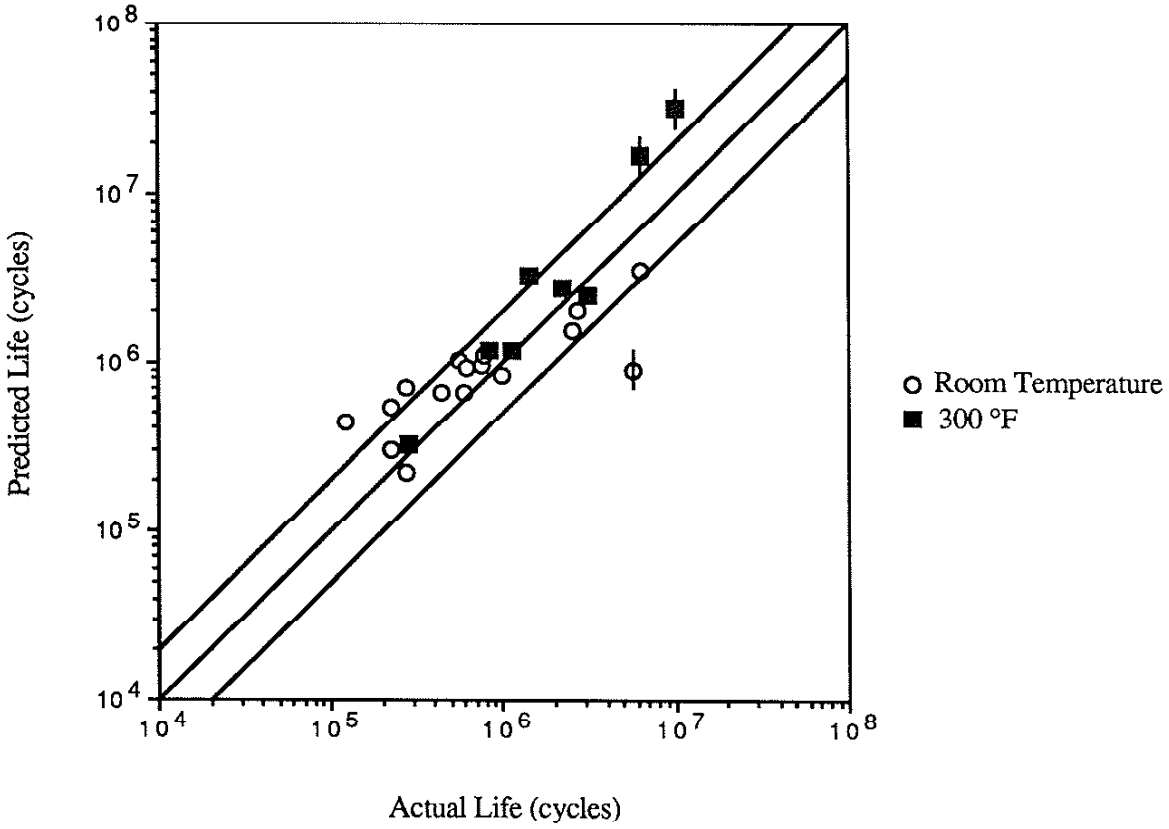

Fig. 31 Comparison of the predicted life and the actual life for Lost-Foam Aluminum-Silicon. The lines to the left and right of the predicted = actual line (middle) indicatcs a factor of two. The symbols with the vertical lines indicates grip-end failures.

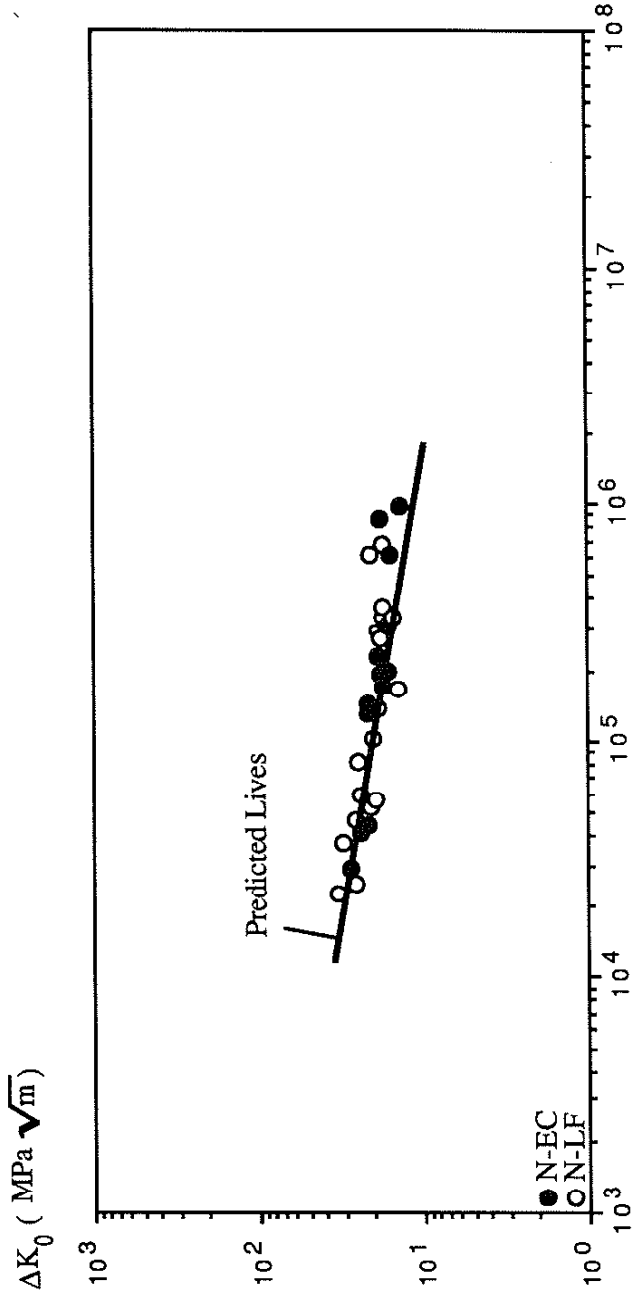

Fig. 32 Comparison of predicted life curves and the graph of stress intensity factor versus cycles to failure curve for nodular cast iron.

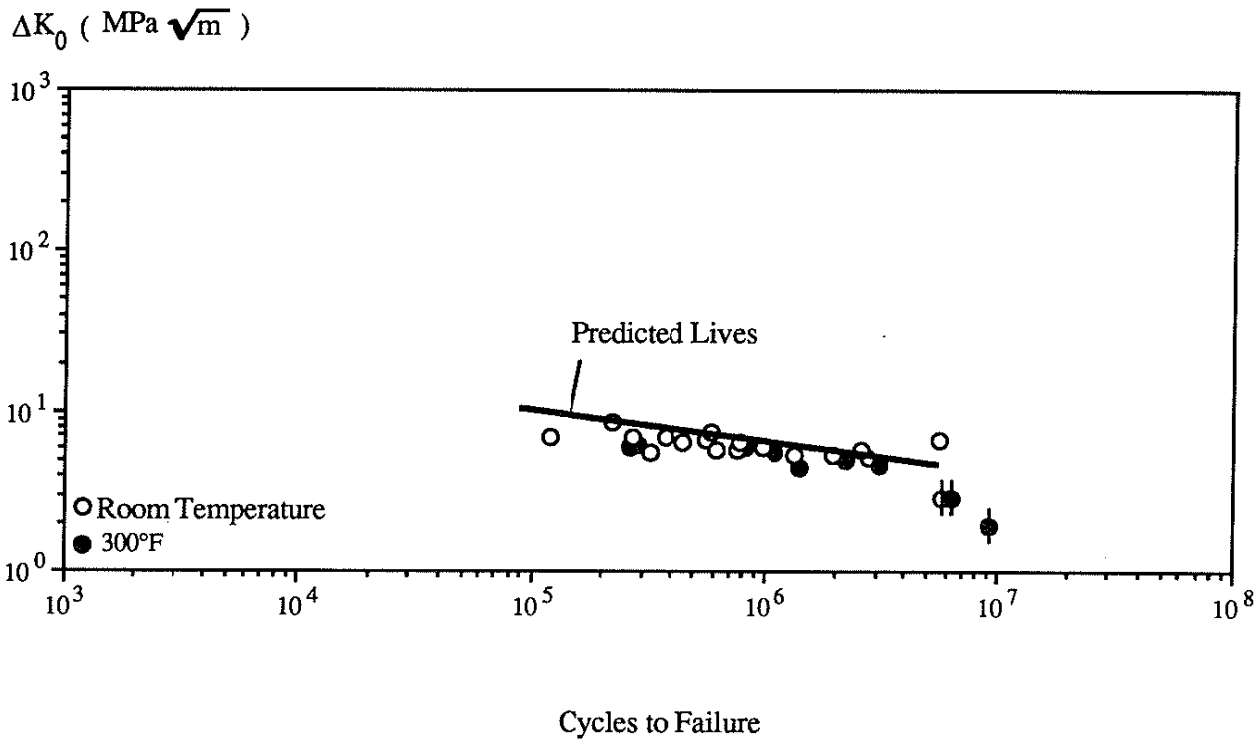

Fig. 33 Comparison of predicted life curve and the graph of Stress intensity factor versus cycles to failure curve for Aluminum-Silicon. A symbol with the vertical line indicates a grip-end failure.

APPENDIX A

Calculation of the Stress Intensity Factors

Semi-Elliptical Surface Flaw in Tension:

The analysis was based on a solution for the stress intensity factor of a mode I semi elliptical flaw in tension (see figure 29).

$$K_I = C^* \sigma \sqrt{\frac{\pi a}{\Phi}} \tag{A1}$$

Where :

$$C^* = \left(C_1 + C_2 \left(\frac{a}{B}\right)^2 + C_3 \left(\frac{a}{B}\right)^4 \right) C_4 \; g(\varphi) \; g(W) \tag{A2}$$

$$C_1 = 1.13 - 0.09\left(\frac{a}{c}\right) \tag{A3}$$

$$C_2 = -0.54 + \frac{0.89}{0.2 + \left(\frac{a}{c}\right)} \tag{A4}$$

$$C_3 = 0.5 - \frac{1.0}{0.65 + \left(\frac{a}{c}\right)} + 14\left(1.0 - \left(\frac{a}{c}\right)\right)^{24} \tag{A5}$$

$$C_4 = 1.0 + \left(0.1 + 0.35\left(\frac{a}{B}\right)^2\right)(1 - \sin\varphi)^2 \tag{A6}$$

$$g(\varphi) = \left(\sin^2\varphi + \left(\frac{a}{c}\right)^2 \cos^2\varphi \right)^{\frac{1}{4}} \tag{A7}$$

$$g(W) = \left(\sec \frac{\pi c}{W} \left(\frac{a}{B}\right)^{\frac{1}{2}} \right)^{\frac{1}{2}} \tag{A8}$$

$$\Phi = \int_0^{\frac{\pi}{2}} \left(1 - \left(\frac{c^2 - a^2}{c^2}\right)\sin^2\varphi\right)^{\frac{1}{2}} d\varphi \qquad \text{(A9)}$$

Equation A9 can be developed into a serial solution with accuracy of better than 5%[23] as follows:

$$\Phi = \frac{\pi}{2}\left(1 - \frac{1}{4}\frac{c^2 - a^2}{c^2} - \frac{3}{64}\left(\frac{c^2 - a^2}{c^2}\right)^2 - \cdots\right) \qquad \text{(A10)}$$

The solution (A1) is valid under the following boundary conditions:

$$0 < \frac{a}{c} < 1$$
$$0 < \frac{a}{B} < 1$$
$$0 < \frac{c}{B} < 1$$
$$0 < \varphi < \pi$$

Embedded Circular Slit Crack:

The stress intensity factor of an internal circular flaw (Type II) were calculated using the following equation:

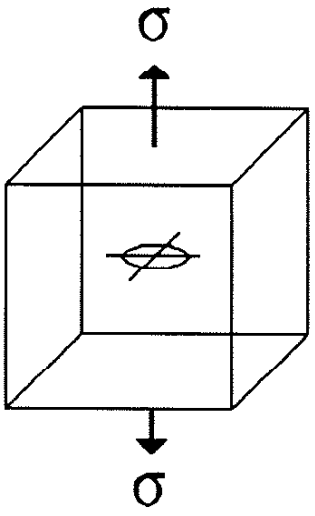

$$K_I = \frac{2}{\pi}\sigma\sqrt{\pi a}$$

where a = the radius of the circular flaw

APPENDIX B

```
c ***********************************************************************
c
c       This Program calculates the value for ΔK for a
c
c    SEMI ELLIPTICAL SURFACE FLAW IN TENSION.
c
c       The equation can be found on page 50 in:
c       Ewalds, Wanhill; Fracture Mechanics; 1986.
c
c
c       Input variables:
c               smax     : Maximum stress (MPa)
c               r        : load ratio, R = 0.1
c               aspect   : aspect ratio; assumed to be constant
c               diameter : diameter of specimen cross-section (inches)
c               a        : crack depth (millimeters)
c
c
c
c     Anthony Biell;  December 7, 1988
c
c
c ***********************************************************************
c
c
        program semi
c               sa is the value of phi
     parameter(sa=0.0,pi=3.141592654)
     real kmax,kmin
        real init,m
        open(unit=17,file='dk.out',status='new',iostat=io)
c
        write(*,*)'This program calculates DK.'
        write(*,*)
        write(*,*)'SEMI ELLIPTICAL SURFACE FLAW IN TENSION'
        write(*,*)
        write(*,*)'Hit CR to run program...'
        pause
c
10      write(*,*) 'enter the value for the Smax in MPa'
        read(*,*) smax
c       smax = 482.65
c     write(*,*) 'Enter the value for the load ratio...'
c       read(*,*)r
           r = 0.1
     write(*,*) 'Enter the value for the aspect ratio...'
       read(*,*)aspect
     write(*,*) 'Enter the value for the diameter in inches...'
       read(*,*)diameter
c ** convert to meters **
          diameter = diameter * 0.0254
```

```
c
20      write(*,*) 'enter the value of a in mm'
        write(*,*) '(1000 to quit or 2000 to start over)'
                read(*,*) a
                if(a.ge.1500) then
                        goto 10
                elseif(a.ge.500) then
                        goto 1000
                endif
                a = a/1000
                c = a/aspect
c
    w=(diameter/2)*(pi**.5)
        b=w
c
c     calculate the division to be used in expression
c
           adb=a/b
           adc=a/c
           cdw=c/w
c       c will be used as another constant
c
c
c      calculate C1,C2,C3,C4,g(sa),g(w)
c
c ***********************************************************************
        phi1=(c**2-a**2)/c**2
        phi=(pi/2)*(1-.25*phi1-(3/64)*phi1**2)
        c1=1.13-.09*adc
        c2=-.54+.89/(.2+adc)
        c3=.5-1/(.65+adc)+14*(1-adc)**24
        c4=1+(.1+.35*(adb)**2)*(1-sin(sa))**2
        gfii=((sin(sa))**2+(adc**2)*(cos(sa))**2)**.25
        gw=(1/(cos(pi*cdw)*(adb)**.5))**.5
        c=(c1+c2*(adb)**2+c3*(adb)**4)*c4*gfii*gw
        kmax=c*smax*(pi*a)**.5/phi
        kmin=r*kmax
        dk=kmax-kmin
c
c
100     write(*,*) 'a = ', a
        write(17,*) dk
        write(*,*) 'dK = ',dk
        write(*,*)
                goto 20
1000    stop
        end
```

APPENDIX C

```
c ***********************************************************************
c
c This program calculates the value of da/dN from the inputted
c     N and a read from the file 'na.dat'.  This file is in the form :
c     N a (i.e.,  45000 .00312  ).  The calculation of da/dN is
c     based on the INCREMENTAL POLYNOMIAL METHOD which can be
c     found in the ASTM standard E647 Appendix.  The method involves
c     fitting a second-order polynomial to sets of (2n+1) successive
c     data points, where n is usually 1,2,3 or 4.  It is customary
c     to choose n=3 but a smaller amount of data points might
c     restrict n to be 2.
c
c     Documentation and organization by Anthony Biell, 12-20-88
c     Program written by Mohammed Swellam, Spring 1988
c
c ***********************************************************************
c
c
      program sevenfit
      parameter(maxnd=40)
      dimension x(maxnd),y(maxnd),a(3,4),xx(3)
       open(unit=17,file='na.dat',status='old',iostat=io)
       open(unit=16,file='sevenfit.out',status='new',iostat=io)
       open(unit=18,file='dadn.out',status='new',iostat=io)
          rewind 16
          rewind 17
          rewind 18

c
      i=1
 12    read(17,*,end=15)read1,read2
            x(i)=read1
            y(i)=read2
            i=i+1
            if(i.gt.maxnd) then
                  write(6,*) 'The # of points exceeds the maximum'
                  write(6,*) 'Change the value in the'
                  write(6,*) ' parameter line'
                  stop
            endif
      goto 12
 15    nd=i-1
c
c
c
c
      do 100 i=1,nd-7+1
            j=i+6
            sx=0.0
            sx2=0.0
```

```
            sx3=0.0
            sx4=0.0
            sy=0.0
            sxy=0.0
            sx2y=0.0
                 do 20 l=i,j
                      sx=sx+x(l)
                      sx2=sx2+x(l)**2
                      sx3=sx3+x(l)**3
                      sx4=sx4+x(l)**4
                      sy=sy+y(l)
                      sxy=sxy+y(l)*x(l)
                      sx2y=sx2y+y(l)*x(l)**2
20                 continue
            a(1,1)=j-i+1
            a(1,2)=sx
            a(1,3)=sx2
            a(2,1)=sx
            a(2,2)=sx2
            a(2,3)=sx3
            a(3,1)=sx2
            a(3,2)=sx3
            a(3,3)=sx4
            a(1,4)=sy
            a(2,4)=sxy
            a(3,4)=sx2y
c
c     solving the equations for the ploynomial constants
c
            call sub1(a,3,xx)
            a0=xx(1)
            a1=xx(2)
            a2=xx(3)
            dadn=a1+2*a2*x(i+3)
               write(16,30)I
               write(16,35)a0,a1,a2
               write(16,70)y(i+3),dadn
               write(18,*)dadn
100    continue
       close(unit=17)
       close(unit=16)
       close(unit=18)
c
c
30      format(///2X,'RESULTS FOR THE FITTING OPERATION #',I2)
35        format(/2x,'a0=',e20.9,/,2x,'a1=',e20.9,/,2x,'a2=',e20.9)
70       format(/5x,'crack length=',f8.6,5x,'da/dN=',f12.10)
c
c
           write(6,*) 'PROGRAM SEVENFIT COMPLETE'
       stop
       end
c
c
c      ------------------------------------------------------
```

```
c
c     ***  subroutine sub1  (called from sevenfit)  ***
c
c     ------------------------------------------------------
c
      subroutine sub1(a,n,z)
      dimension a(3,4),z(3)
      do 80 k=1,n
           c=a(k,k)
           do 30 j=k,n+1
                a(k,j)=a(k,j)/c
30         continue
           do 75 i=1,n
                if(i.eq.k) then
                     goto 75
                endif
                c=-a(i,k)
                do 60 j=k,n+1
                     a(i,j)=a(i,j)+c*a(k,j)
60              continue
75         continue
80    continue
      z(1)=a(1,n+1)
      z(2)=a(2,n+1)
      z(3)=a(3,n+1)
c
c
      return
      end
```